INTERNATIONAL JOURNAL OF PAVEMENT ENGINEERING
2024, VOL. 25, NO. 1, 2424381
https://doi.org/10.1080/10298436.2024.2424381

Quantifying the impact of chemical composition on pervious concrete strength: a comparative analysis using full quadratic model and artificial neural network

Navaratnarajah Sathiparan [a], Pratheeba Jeyananthan [b] and Daniel Niruban Subramaniam [a]

[a]Department of Civil Engineering, Faculty of Engineering, University of Jaffna, Jaffna, Sri Lanka; [b]Department of Computer Engineering, Faculty of Engineering, University of Jaffna, Jaffna, Sri Lanka

ABSTRACT
The present study investigates the effect of the total amount of chemical constituents in cement and supplementary cementitious materials on the compressive strength of pervious concrete. Experimental datasets were collected from the literature on different types of pervious concrete specimens modified with supplementary cementitious materials. A total of 659 data observations were collected. These were then analysed and modelled using three different approaches: linear regression (LR), full quadratic (FQ) and artificial neural network (ANN) models. These models' purpose was to predict pervious concrete's compressive strength. The accuracy of the models was evaluated using correlation coefficient (R^2), root mean square error (RMSE), mean absolute error (MAE), a-20 index and error distribution. The ANN model demonstrated superior effectiveness and accuracy in predicting the compressive strength of pervious concrete, as indicated by the performance metrics. The analysis results showed that Al_2O_3 content and curing time were the most influential parameters in predicting the compressive strength of concrete. In addition, SHapley Additive exPlanations (SHAP) analysis could determine if each input variable had a positive or negative effect on compressive strength. Al_2O_3, CaO, curing time and water content positively affected the compressive strength of pervious concrete, while SiO_2 and corresponding alkalis had a negative effect.

ARTICLE HISTORY
Received 29 April 2024
Accepted 26 October 2024

KEYWORDS
Pervious concrete; supplementary cementitious materials; compressive strength; ANN; full quadratic

1. Introduction

Pervious concrete is a particular type of concrete with high porosity that allows water to pass through. It is made with minimal fine aggregates (sand) and a higher proportion of coarse aggregates (gravel or crushed stone), which creates interconnected voids within pervious concrete (Elango *et al.* 2021). Applications for pervious concrete include stormwater management, erosion control, groundwater recharge and car parks. Pervious concrete helps reduce stormwater runoff that can carry pollutants such as oil, heavy metals and sediment into rivers, lakes and oceans. By allowing water to soak into the ground, pervious concrete helps filter pollutants and improve water quality (Subramaniam and Sathiparan 2023). It also has higher reflectivity and lower heat absorption than traditional asphalt paving, efficiently reducing the urban heat island effect and lowering ambient temperatures in urban areas.

Pervious concrete typically requires more cement than conventional concrete as it contains lower proportion of fine aggregates (sand), generally used to fill voids and provide cohesion in traditional concrete mixes. In pervious concrete, the voids are intentionally incorporated to allow water to pass through, so a higher cement content is needed to ensure adequate strength and durability (Sathiparan *et al.* 2024). Additionally, special admixtures may be added to pervious concrete mixes to improve workability and enhance its permeability characteristics. However, using excessive cement in construction can contribute to several environmental issues. Cement production is a dominant source of carbon dioxide (CO_2) emissions contributing to climate change. The production of cement requires limestone and other materials to be heated to high temperatures, releasing CO_2. Cement production is also energy intensive, requiring large amounts of energy to heat kilns and grind raw materials (Mokhtar and Nasooti 2020). Excessive cement consumption exacerbates energy demand, much of which comes from non-renewable sources, leading to increased greenhouse gas emissions and resource depletion (Sathiparan 2021). Therefore, researchers working on alternatives to cement in construction include fly ash, metakaolin, silica fume, rice husk ash, ground granulated blast furnace slag, etc. Also, researchers explore alternative binder materials, such as geopolymers and calcium sulfoaluminate cement, which have lower carbon footprints than Portland cement (Althoey *et al.* 2023). These supplementary cement materials (SCMs) and alternative binders can decrease the environmental impact of construction materials while maintaining performance and durability.

When supplementary cement materials were used in pervious concrete, the characteristics of pervious concrete depended on SCM replacement level and on factors such as chemical composition of SCMs, aggregate-to-cement ratio, fine content, water-to-cement ratio, curing period, etc. (Chindaprasirt *et al.* 2008, Chen *et al.* 2024). Therefore, a prediction model for properties of pervious concrete is essential for

CONTACT Navaratnarajah Sathiparan nsakthiparan@yahoo.com

ensuring the structural integrity and performance of pervious concrete pavements and other applications. These models can help engineers and researchers estimate the strength of pervious concrete mixes based on their constituents and proportions (Singh *et al.* 2023b). Several prediction models have been developed: empirical models, mechanistic-empirical models**,** artificial neural networks (ANNs) and machine learning algorithms (Wijekoon *et al.* 2024). These prediction models serve as valuable tools for engineers and researchers to optimise mix designs, evaluate the effects of different factors on compressive strength, and ensure the quality and durability of pervious concrete structures. Also, some research focuses on predicting the compressive strength of pervious concrete using non-destructive methods such as ultrasonic pulse velocity and electrical resistivity (Singh *et al.* 2023a, Sathiparan *et al.* 2024b).

ANN and machine learning models excel over empirical and mechanistic-empirical models' counterparts due to their capability to handle complex, non-linear associations in data, leveraging vast datasets for accurate predictions (Almeida 2002). They adapt to various input types, scale for large datasets, and automatically select relevant features, saving time and reducing bias. Ensemble methods further enhance accuracy by combining multiple models. Machine learning's robustness to noise ensures reliability in real-world scenarios (Yaqoob *et al.* 2023). However, challenges include the need for representative sample observations of the population, guarding against overfitting and interpreting results (Sarker 2021). Machine learning offers versatile, data-driven approaches for predicting the compressive strength of pervious concrete that also assess the model's validity and interpretability.

Table 1 summarises the machine learning prediction models for the compressive strength of pervious concrete. Several studies have explored machine learning to predict the compressive strength of pervious concrete blended SCMs like fly ash and silica fume. eXtreme Gradient Boosting (XGBoost) and ANN are often the top performers, achieving high accuracy. Support Vector Regression (SVR) and random forest also show good performance, capable of exceeding the accuracy of other methods like ANNs in some cases. Other basic models, such as linear regression, multi-layer Perceptron (MLP) and so on, are also explored, but often with lower accuracy than the above.

Table 1. Summary of the machine learning prediction models for compressive strength of SCMs blended pervious concrete.

Refs.	SCMs used	ML used	No. of data	Best ML model	Accuracy
Sathiparan *et al.* 2023	Fly ash	LR, ANN, BDT, RF, SVR, XGB	437	XGB	$R^2 = 0.98$ RMSE = 1.62 MPa
Sathiparan *et al.* 2024a	Silica fume	LR, ANN, BDT, KNN, RF, SVR, XGB	222	XGB	$R^2 = 0.99$ RMSE = 0.28 MPa
Ahmad *et al.* 2024	Waste glass powder	LR, NLR, ANN	99	ANN	$R^2 = 0.99$ RMSE = 0.53 MPa
Le *et al.* 2022	Silica fume	ANN, SVR, XGB	164	XGB	$R^2 = 0.92$
Sudhir Kumar *et al.* 2024	Ground Granulated Blast furnace Slag	MLR, ANN	36	ANN	$R^2 = 0.99$ RMSE = 0.13 MPa

LR: linear regression, NLR: non-linear regression, MLR: multi-linear model, ANN: artificial neural network, BDT: boosted decision tree regression, KNN: K-nearest neighbours, RF: random forest regression, XGB: eXtreme gradient boosting.

There are several limitations to using a machine learning model, such as limited data availability, model interpretability, standardisation and practical implementation. Existing studies often use datasets from the literature, which may not be comprehensive or readily available (Stadlhofer and Mezhuyev 2023). While some models like Random Forest and XGBoost offer decent interpretability, they are more like black boxes. So, additional work would be needed to understand the internal mechanisms of complex models for more logical interpretation, application and control (Zhang *et al.* 2022, Parimbelli *et al.* 2023). The lack of standardised testing procedures and mixed design methodologies often make comparison of results across studies and training robust models more challenging. Also, integrating these models into construction practices and design workflows requires user-friendly interfaces and clear guidelines for interpretation and uncertainty quantification.

These past studies used SCM replacement levels in addition to some mix parameters and curing periods for the prediction of the compressive strength of pervious concrete with the inclusion of a single SCM. The strength of pervious concrete depends not only on mix parameters and curing period but is also highly influenced by the material properties of cementitious materials, especially chemical composition (Shen *et al.* 2021). SCMs typically contain amorphous silica (SiO_2), alumina (Al_2O_3), icon (Fe_2O_3) and magnesium (MgO), which react with calcium hydroxide ($Ca(OH)_2$) liberated during cement hydration to form additional calcium silicate hydrate (C-S-H), calcium aluminate hydrate (C-A-H), calcium iron aluminate hydrate (C-A-F-H) and magnesium calcium hydroxide hydrate (Mg-CH) gel, respectively (Rivas Mercury *et al.* 2006, Gong and White 2021, Alventosa *et al.* 2022). This pozzolanic reaction leads to denser microstructure and improved strength development with time. On the other hand, SCMs can chemically bind specific ions, such as alkalis and sulfates, which can, on the contrary, lead to deleterious reactions and reduce concrete strength with time (Von Greve-Dierfeld *et al.* 2020, Kaladharan *et al.* 2021). Certain SCMs, such as fly ash, can mitigate the risk of Alkali–silica reaction by consuming reactive silica in the concrete mixture, thereby preventing the formation of expansive gel and subsequent cracking (Hay and Ostertag 2021). Although several studies focus on how the chemical composition of SCMs affects the strength of pervious concrete, the prediction model based on the overall chemical composition in the pervious concrete mix and their influence on predicting pervious concrete's compressive strength is scarce in published literature.

This study, therefore, proposes a prediction model for the compressive strength of pervious concrete based on the chemical composition of the mix, mix design parameters, aggregate size and curing period. Observations were collected from the published literature, and three mathematical models, namely linear regression, full quadratic and ANN models, are proposed for prediction of compressive strength. As ensuring adequate compressive strength remains crucial for pervious concrete pavements to withstand traffic loads and maintain long-term performance, developed models in this study offer valuable tools for pavement engineers. By enabling the prediction of pervious concrete strength based on readily available compositional data, ultimately aiding in the design and optimisation of pavements utilising this sustainable material.

2. Methodology

2.1. Data collection

A systematic literature review was undertaken, following the PRISMA methodology. Searching and collecting research articles was carried out using the SCOPUS database, supplemented by searches made on Google Scholar. A search query was conducted on the SCOPUS database using article title, abstract and keywords. The search was performed using the following keywords: 'pervious concrete', 'pervious concrete', 'porous concrete', 'supplementary cementitious material', 'fly ash', 'metakaolin', 'rice husk ash', 'granulated blast furnace slag', 'silica fume', 'limestone', 'glass powder', 'palm oil fuel ash', and 'sorghum husk ash'. Afterwards, the literature was examined to avoid any repetition of data. After going through the articles, articles without details about chemical composition of SCMs and the mix design detail were excluded from further analysis.

After initial screening, 32 entries were retrieved from SCOPUS database and Google Scholar. Several studies used admixtures to enhance strength characteristics and the strength dominantly depended on the quantity of admixtures and type of admixtures used. Yet, a clear description of the kind of admixture used in these studies is required to be studied. Therefore, these studies with insufficient details were removed from further analysis. Similarly, few studies used fine aggregates with various sizes for mix design. Having yet to establish the impact of the size of fines on strength, these studies were also excluded in subsequent analyses. The final sample matrix comprised of 659 observations from 20 published literature that comprehensively explored usage of SCMs in the context of pervious concrete, which are summarised in Table 2. The amount of published literature using fly ash, rice husk ash, glass powder and metakaolin as cement substitutes in pervious concrete is seen substantial. All tests were done on specimens prepared in the laboratory.

From published literature listed in Table 2, calcium oxide (CaO), silicon dioxide (SiO_2), ferric oxide (Fe_2O_3), aluminium (Al_2O_3), magnesium oxide (MgO), equivalent alkali, aggregate content, water content, aggregate size, curing period and corresponding compressive strength were extracted. The chosen parameters are crucial to understanding the hydration process and microstructure of pervious concrete, which significantly influences its compressive strength. It is essential to recognise how these factors specifically relate to the unique characteristics of pervious concrete compared to conventional concrete.

- CaO content: In pervious concrete, CaO is vital as it reacts with water to form calcium silicate hydrate (C-S-H), the key binding agent. Higher CaO content typically enhances strength by promoting a denser C-S-H matrix. However, in pervious concrete, an optimal balance must be maintained to ensure adequate porosity for water drainage, as excessive CaO can lead to a denser structure that may compromise permeability (Harrisson 2019).
- SiO_2 content: SiO_2 is integral in forming C-S-H when combined with CaO. In pervious concrete, achieving the right CaO/SiO_2 ratio is particularly important. An optimal ratio not only strengthens the C-S-H gel but also helps maintain the necessary void structure for permeability, critical for applications requiring water drainage (He *et al.* 2014).
- Al_2O_3 content: While Al_2O_3 can enhance strength in pervious concrete by contributing to C-S-H formation, high levels may slow hydration, affecting the early strength gain essential for structural integrity. This is crucial in pervious applications where rapid strength development is desired to withstand traffic loads (Baltakys *et al.* 2019).
- Fe_2O_3 content: In small quantities, Fe_2O_3 may enhance the mechanical properties of pervious concrete. However, excessive Fe_2O_3 can adversely affect strength and setting time, which is critical for ensuring quick setting in environments where drainage is essential (Najafi Kani *et al.* 2021).
- MgO content: MgO contributes minimally to strength in pervious concrete, primarily filling voids. High MgO levels can slow down hydration, leading to delays in strength development. This is a consideration in designing mixtures that require timely strength for immediate use (Hillier 2007).
- Equivalent alkali content: The combined effect of alkali oxides (Na_2O & K_2O) can impact the formation of expansive alkali–silica gel, potentially leading to cracking in pervious concrete. Managing alkali content is crucial to maintaining both strength and permeability, as uncontrolled expansion can compromise the material's performance (Hillier 2007).
- Aggregate content: In pervious concrete, the ratio of aggregate to binder is critical. While higher aggregate content can reduce the binding agent's availability, it is necessary to ensure sufficient porosity for drainage. This balance directly influences the overall strength and durability of the concrete.
- Water content: Adequate water is essential for hydration, but excessive water can create a porous structure that reduces strength. Establishing an optimal water-to-cement (w/c) ratio is particularly vital in pervious concrete to ensure both effective hydration and the desired drainage properties.
- Aggregate size: The distribution of aggregate sizes affects packing density and the amount of binder required in pervious concrete. Larger aggregates can increase porosity, potentially decreasing strength if not offset by adjustments in the binder content. This aspect is crucial for maintaining the necessary voids for water flow.
- Curing period: Proper curing is essential for the strength development of pervious concrete. Longer curing times that maintain moisture and temperature can significantly enhance strength through continued hydration. This is

Table 2. Literature list used for collection of datasets.

SCMs	No. of articles	Reference	Specimen shape	Size of the specimen[1]	Standard used	No. of data
Fly ash	8	Tan and Du 2013	Cubic	100 mm	BS EN 12390-3 (2019)	24
		Prajapati *et al.* 2019	Cubic	150 mm	IS: 516 (1959)	8
		Singh *et al.* 2022	Cubic	150 mm	IS: 516 (1959)	15
		Hwang and Yeon 2022	Cylindrical	100 mm × 200 mm	ASTM C39 (2021)	30
		Boddu 2023	Cubic	150 mm	ASTM C39 (2021)	9
		Kumar and Srikanth 2023	Cylindrical	100 mm × 200 mm	IS: 516 (1959)	3
		Nazeer *et al.* 2023	Cubic	150 mm	IS: 516 (1959)	12
		Subramaniam and Sathiparan 2023	Cubic	150 mm	ASTM-C109 (2020)	40
Metakaolin	2	Singh *et al.* 2022	Cubic	150 mm	IS: 516 (1959)	15
		Rama and Shanthi 2023	Cubic	150 mm	IS: 516 (1959)	16
Rice husk ash	2	Talsania *et al.* 2015a	Cubic	150 mm	IS: 516 (1959)	27
		Subramaniam and Sathiparan 2023	Cubic	150 mm	ASTM-C109 (2020)	32
GGBS	2	El-Hassan and Kianmehr 2017	Cylindrical	150 mm × 300 mm	ASTM C39 (2021)	20
		Sudhir Kumar *et al.* 2024	Cubic	150 mm	IS: 516 (1959)	36
POFA	1	Khankhaje *et al.* 2018	Cylindrical	100 mm × 200 mm	ASTM C39 (2021)	10
SHA	2	Tijani *et al.* 2019	Cylindrical	100 mm × 200 mm	ASTM C39 (2021)	18
		Tijani *et al.* 2022	cylindrical	100 mm × 200 mm	ASTM C39 (2021)	18
Glass powder	2	Talsania et al. 2015a	Cubic	150 mm	IS: 516 (1959)	27
		Li *et al.* 2021	Cubic	100 mm	GB/ T50081 (2002)	60
Hypo sludge	1	Talsania *et al.* 2015b	Cubic	150 mm	IS: 516 (1959)	27
Truss	1	Joshaghani *et al.* 2015	Cylindrical	100 mm × 200 mm	ASTM C39 (2021)	48
Calcium carbide & RHA	1	Adamu *et al.* 2021	Cubic	100 mm	BS EN 12390 4 (2019)	42
Nano-clay & pumice powder	1	Mehrabi *et al.* 2021	Cylindrical	100 mm × 200 mm	ASTM C39 (2021)	120
Fly ash & silica fume	1	Nazeer *et al.* 2023	Cubic	150 mm	IS: 516 (1959)	12

[1]For cubic specimens, side dimension and for cylindrical specimens, enter the diameter × height.

especially important in applications where structural performance is required shortly after placement.

These parameters are interrelated and influence hydration process, formation of microstructure, and ultimately affect compressive strength of pervious concrete. By considering these factors and their interactions, models can be developed to predict expected compressive strength for different SCM-blended pervious concrete mixtures. Calcium oxide content in the mix is calculated in Equation (1).

$$\mathrm{CaO}\left(\mathrm{in}\,\frac{\mathrm{kg}}{\mathrm{m}^3}\right) = (\mathrm{C}_{\mathrm{cement}} \quad \mathrm{CaO}_{\mathrm{cement}}/100) \quad \mathop{}_{i=1}^{n} (\mathrm{C}_{\mathrm{SCM}_i} \quad \mathrm{CaO}_{\mathrm{SCM}_i}/100) \tag{1}$$

where C_{cement}: cement content in the mix (kg/m^3), C_{SCM}: one particular SCM content in the mix (kg/m^3), i: ith number of SCM, n: number of SCMs in the mix, CaO_{cement}: CaO content in cement in percentage and CaO_{SCM}: CaO content in SCM in percentage.

Similarly, other chemical components in the mix were also calculated based on Equation (1) with CaO replaced with a particular chemical component. The equivalent alkali content is determined by adding the amount of sodium oxide to the converted amount of potassium oxide (Na_2O+0.658 K_2O). Aggregate content and water content were measured in kg/m^3. The aggregate size and curing period were measured in mm and days, respectively.

Figure 1 illustrates the distribution of variables contained within the dataset. Data shown demonstrates the range of CaO, SiO_2, Al_2O_3, Fe_2O_3, MgO, equivalent alkalies, coarse aggregate and water content from 123.6 to 384.5, 47.0–178.7, 8.5–99.2, 1.9–66.0, 2.5–21.2, 0–12.9, 689.0–1833.6 and 75.6–265.0 kg/m^3, respectively. In addition, aggregate size varied from 5 to 20 mm, while curing period varied between 1 and 120 days. The present study included an extensive dataset on characteristics of pervious concrete, which is expected to have practical applications in several industrial settings. Additionally, it is essential to mention that all parameters except aggregate content had positive skewness values.

2.2. Mathematical and ANN models

Figure 2 depicts flowchart that demonstrates the utilisation of mathematical and ANN model for predicting compressive strength of pervious concrete. Initial stage entails the preparation of dataset. Dataset includes values of 659 independent and dependent variables. Participants were randomly assigned to two groups. Two-thirds of the dataset were utilised to train the model, creating a training dataset. A portion equivalent to one-third of the dataset was put aside to evaluate performance of the model, thereby forming test (validation) dataset. Linear regression, full quadratic and ANN models were trained in the second stage using provided dataset. Prior to ANN implementation, hyperparameter optimisation was utilised to optimise parameters of machine learning algorithms. Given extensive variety of possible combinations, this research concentrated on frequently recorded hyperparameter ranges. The performance of each model was assessed on both training and test datasets using R^2 and RMSE values to prevent overfitting. In validation stage, testing dataset was used to confirm the accuracy and efficiency of the model created.

Subsequently, predictions generated by the models were compared to actual measured values. The performance of all models was thoroughly evaluated using four performance metrics: R^2, RMSE, MAE and a20 index. The α20-index is a novel metric employed to assess the dependability of a well-established model. Computation entails dividing the number of data points within a predicted strength-to-experimental strength ratio ranging from 0.80 to 1.2 by the total number of data points.

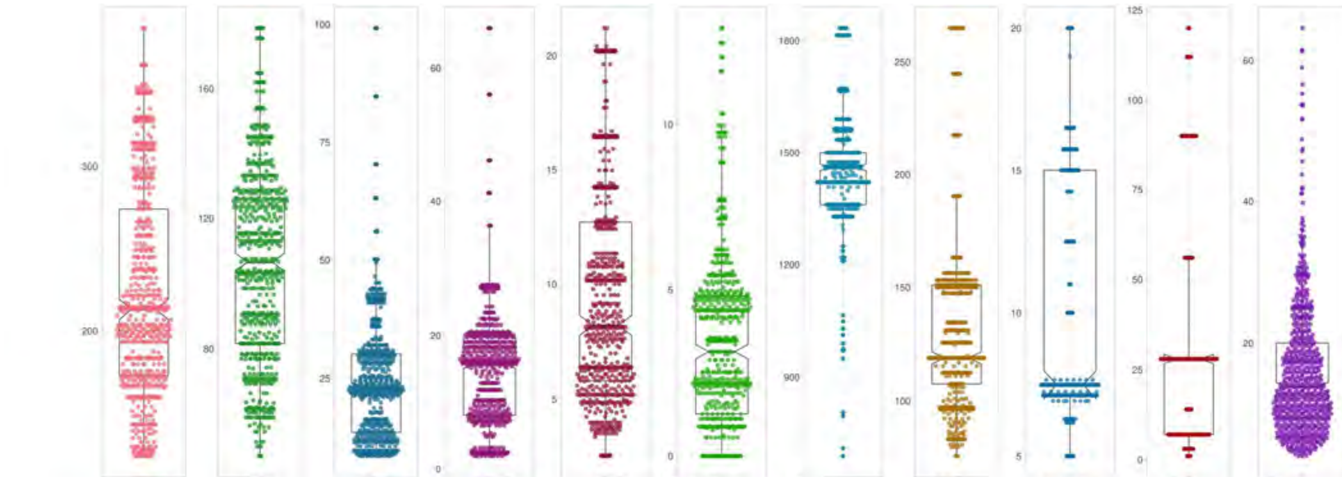

	CaO (kg/m³)	SiO₂ (kg/m³)	Al₂O₃ (kg/m³)	Fe₂O₃ (kg/m³)	MgO (kg/m³)	Equivalent alkalies (kg/m³)	Coarse aggregate (kg/m³)	Water (kg/m³)	Agg. size (mm)	Curing period (days)	Strength (MPa)
Minimum	123.62	47.00	8.54	1.95	2.51	0.00	689.00	75.57	5.00	1.00	4.01
Maximum	384.55	178.66	99.23	65.97	21.21	12.91	1833.60	265.00	20.00	120.00	64.57
Mean	223.68	105.86	25.05	15.25	9.54	3.43	1455.05	137.01	10.08	31.93	16.09
Standard div.	64.52	29.44	14.60	9.81	4.75	2.64	162.55	46.00	4.07	30.24	9.70
Skewness	0.52	0.15	1.93	1.83	0.72	1.03	-0.83	1.44	0.82	1.39	1.78
Kurtosis	-0.70	-0.62	6.06	6.62	-0.40	1.29	4.75	1.60	-0.68	0.87	4.43

Figure 1. Parameter distribution considered in the study.

2.2.1. Linear model

Linear regression (LR) is a statistical technique employed to elucidate linear association between dependent and a combination of independent variables. The procedure entails identifying the most suitable linear regression model that precisely depicts association between dependent and independent variables, as indicated in Equation (2). In this case, variables a_0–a_{10} indicate parameters of the model. While constant a_0 is termed bias, constants a_1–a_{10} are referred to as weights in machine learning models.

$$\mathrm{CS} = a_0 \quad a_1(\mathrm{Ca}) \quad a_2(\mathrm{Si}) \quad a_3(\mathrm{Al}) \quad a_4(\mathrm{Fe}) \quad a_5(\mathrm{Mg}) \quad a_6(\mathrm{Na.E}) \quad a_7(\mathrm{Agg}) \quad a_8(\mathrm{w}) \quad a_9(\mathrm{s}) \quad a_{10}(\mathrm{t}) \tag{2}$$

2.2.2. Quadratic model

Regression models in this study were developed using the response surface method, specifically the quadratic model (FQ), as described by Mao (1981) and Khuri and Ja (1996). Mathematical representation of the model is given by Equation (3).

$$\mathrm{CS} = \beta_0 \quad \sum_{i=1}^{n} \beta_i x_i \quad \sum_{i=1}^{n} \sum_{j=1,\, i\ \ j}^{n} \beta_{ij} x_i x_j \tag{3}$$

In this equation, regression coefficients β_0, β_i and β_{ij} represent arbitrary parameters of regression model. Input variables in the regression function are denoted as x_i and x_j, with a total of n variables in the model. The response variable, compressive strength, is represented as CS. In this study, the number of variables (n) is 10. In quadratic regression, parameters (β_0, β_i and β_{ij}) of the model don't have a direct physical meaning on their own. They represent interplay between independent variable (x_i to x_n) and dependent variable (CS) in the specific context of modelling.

2.2.3. Artificial neural network

An artificial neural network (ANN) is a machine learning model inspired by structure and function of a human brain. The system consists of interconnected synthetic neurons (nodes) organised in layers. Each neuron receives signals from other neurons, processes them using an activation function and sends its output to other connected neurons (Sathiparan and Jeyananthan 2023). Unlike simpler models like linear regression, ANNs can learn complex, non-linear relationships between input and output data. ANNs require the tuning of several hyperparameters to achieve optimal performance. These include a number of hidden layers and neurons, activation functions and learning rates. Figure 3 shows the structure of the ANN model. This study was designed with 10 variables (Ca, Si, Al, Fe, Mg, Na.E, Agg, w, s and t) as input and compressive strength (CS) as output. In the hidden layer, a tanh activation function is utilised.

The output variable is linked with input variables by weights and biases as shown in Equation (4) (Snieder *et al.* 2020).

$$\mathrm{CS} = f\left(\sum_{i=1}^{n} w_i x_i \quad \mathrm{bias}\right) \tag{4}$$

where w_j is the weights, i is the number of input variables, x_j is the input parameters, and bias is the threshold for the tanh function.

2.2.3.1. Performance assessment criteria.

To assess the performance of a prediction model, four different indicators, coefficient of determination (R^2), root mean squared error ($RMSE$), mean absolute error (MAE) and a20 index, are

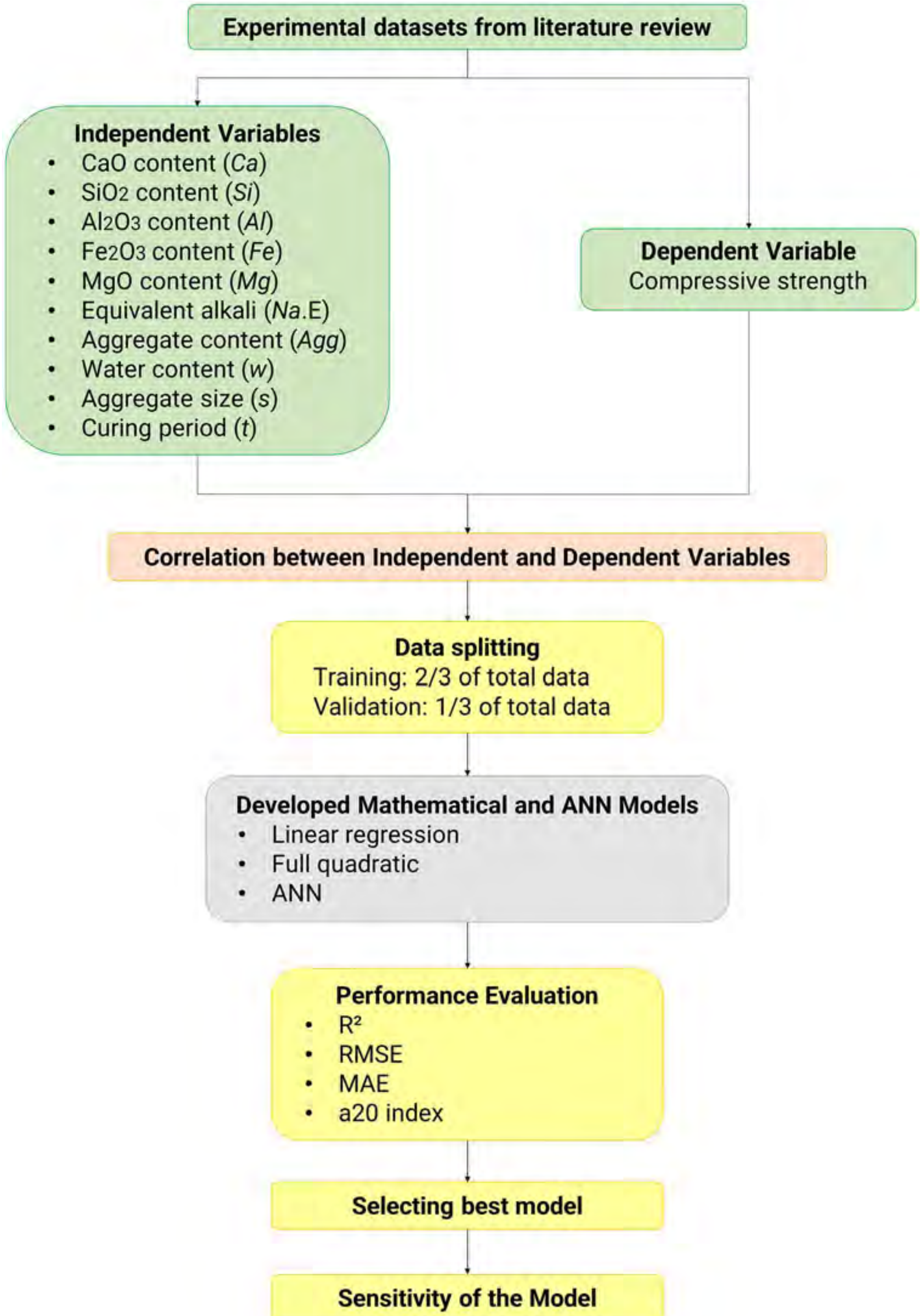

Figure 2. Modeling procedure flow chart.

used, which were defined as Equations (5)–(8).

$$R^2 = 1 - \frac{\sum_{i=1}^{n} (P_i - E_i)^2}{\sum_{i=1}^{n} (E_i - E)^2} \tag{5}$$

$$RMSE = \sqrt{\frac{\sum_{i=1}^{n} (P_i - E_i)^2}{n}} \tag{6}$$

$$MAE = \frac{\sum_{i=1}^{n} P_i - E_i}{n} \tag{7}$$

$$a20_{\text{index}} = \frac{N_{20}}{N} \tag{8}$$

where P_i: predicted value, E_i: experimental value, P: mean of predicted value, E : mean of experimental value, N: total number of datasets, N_{20}: total number of predicted to the measured data of value ratio ranged from 0.8 to 1.2.

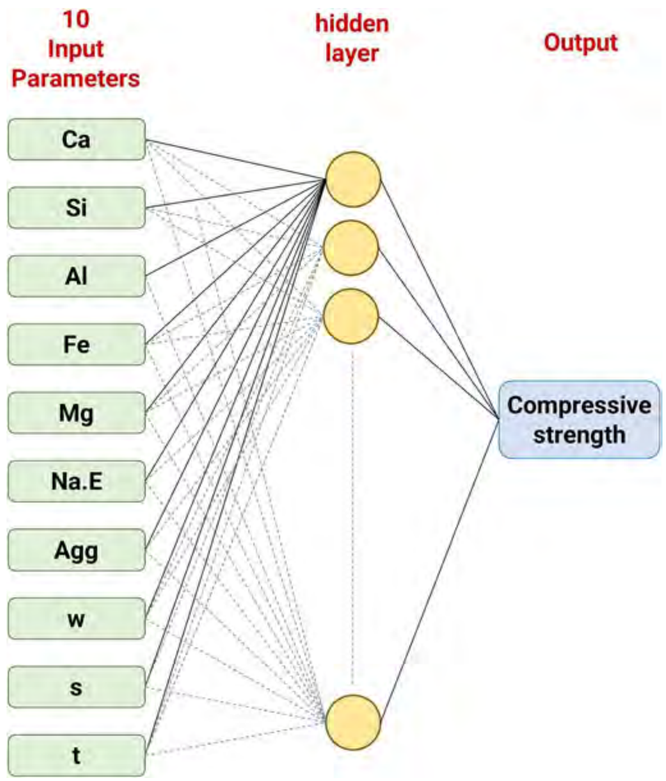

Figure 3. The structure of ANN model.

3. Statistical analysis

Figure 4 illustrates the relationships among chemical, aggregate and water contents. Every cell provides a numerical count ranging from −1 to +1. The count is represented by a colour, with shades of green indicating higher positive numbers. Green shades exhibit a moderate association (correlation indices between 0.51 and 0.85) among CaO, SiO_2, Al_2O_3, Fe_2O_3 and water concentrations. Binder-to-aggregate ratio is expected to increase all these chemical compositions simultaneously. Also, higher binder content required more water for the mix. The Al_2O_3 and Fe_2O_3 contents exhibit highly significant linear association, indicated by a correlation coefficient of 0.85. Despite a modest negative correlation index, the coarse content showed limited association with other measures.

The influence of each input variable on compressive strength is shown in Figure 5. There is an increasing trend of compressive strength with chemical components (especially CaO, SiO_2, Al_2O_3, Fe_2O_3), water content and curing period. Conversely, compressive strength decreased in trend with an increase in coarse aggregate content and aggregate size. However, the correction between input variable and compressive strength was not significant. Correlation coefficient for compressive strength with parameters CaO, SiO_2, Al_2O_3, Fe_2O_3, MgO, equivalent alkalies, aggregate content, water content, aggregate size and curing period is 0.27, 0.41, 0.54, 0.48, 0.15, 0.03, −0.02, 0.41, −0.30 and 0.38, respectively. These

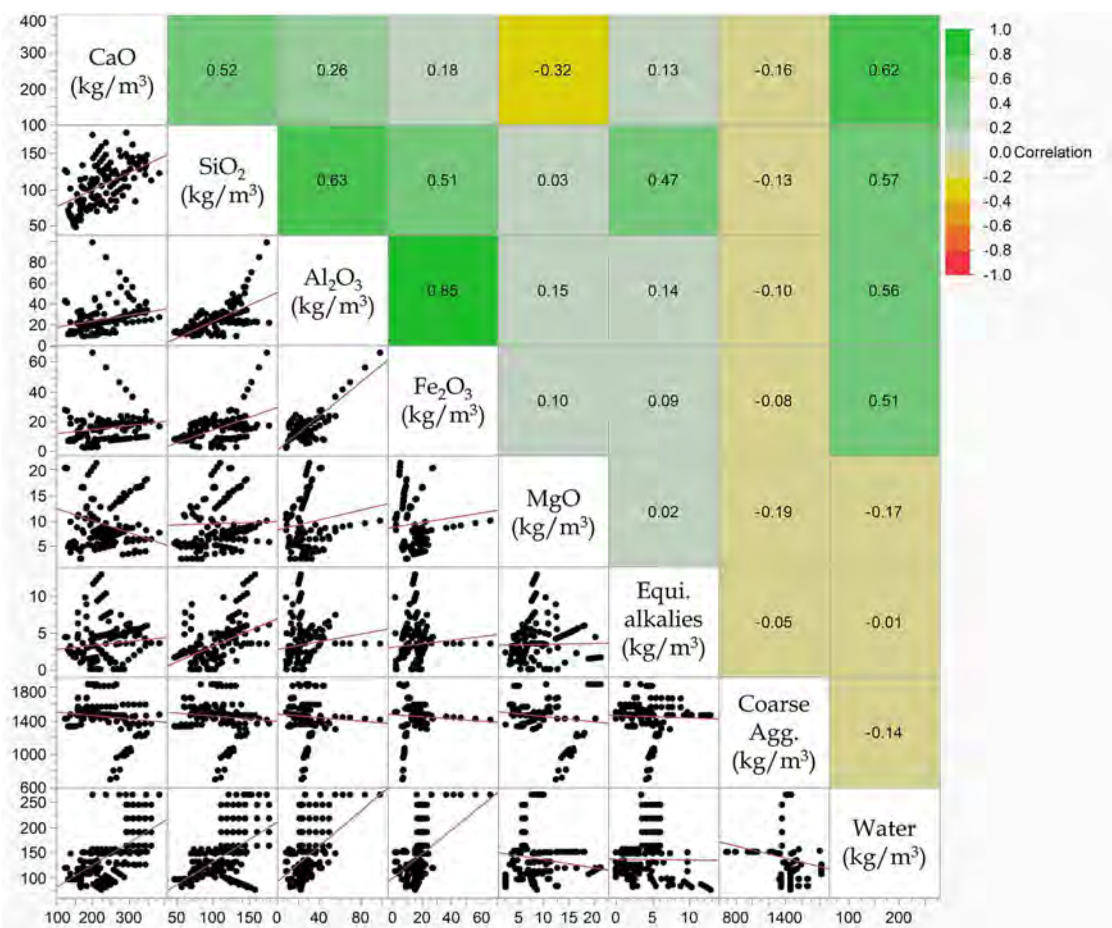

Figure 4. Correlation graph and data heatmap of selected input parameter (aggregate size and curing period are excluded).

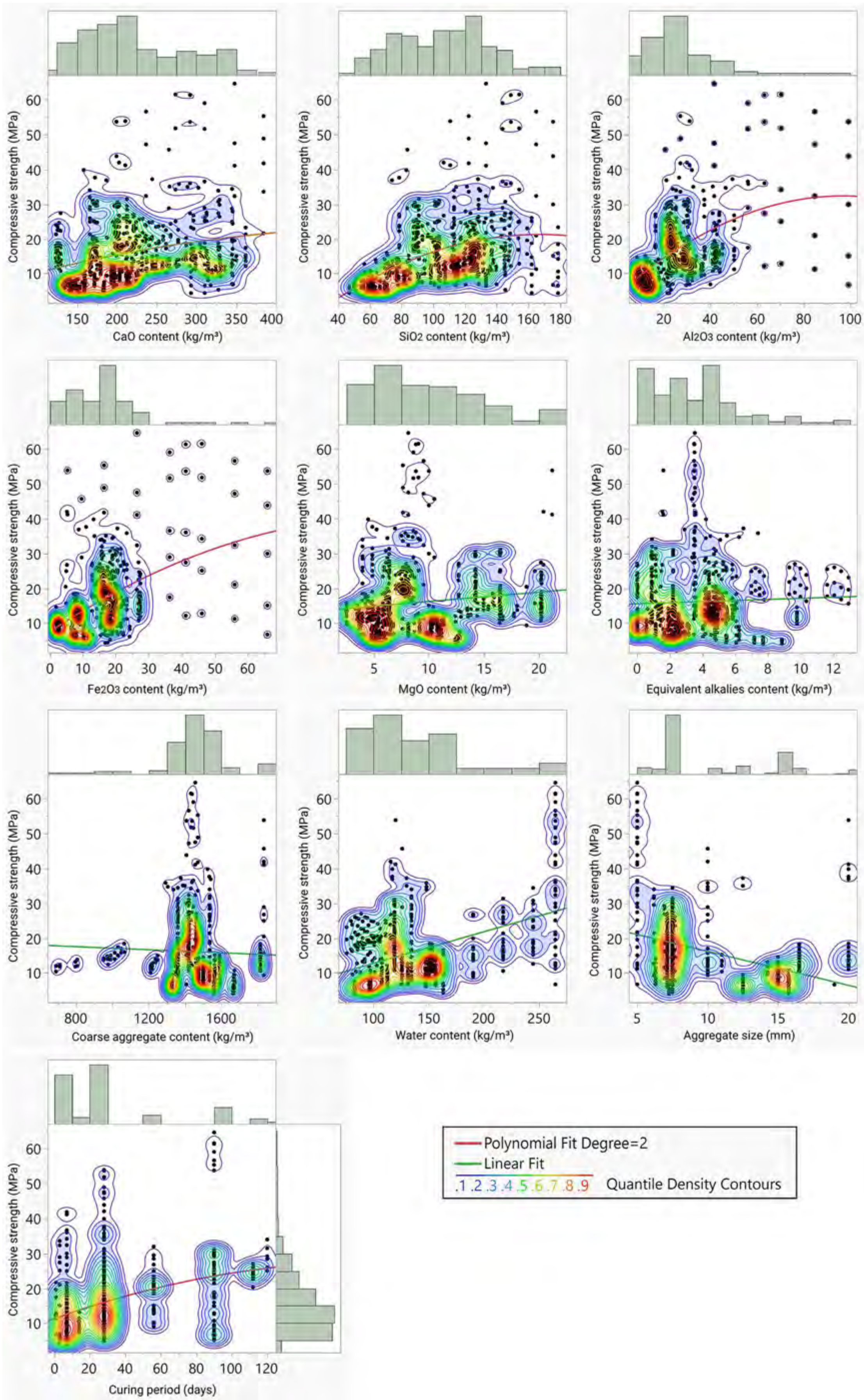

Figure 5. Correlation between compressive strength and input parameters.

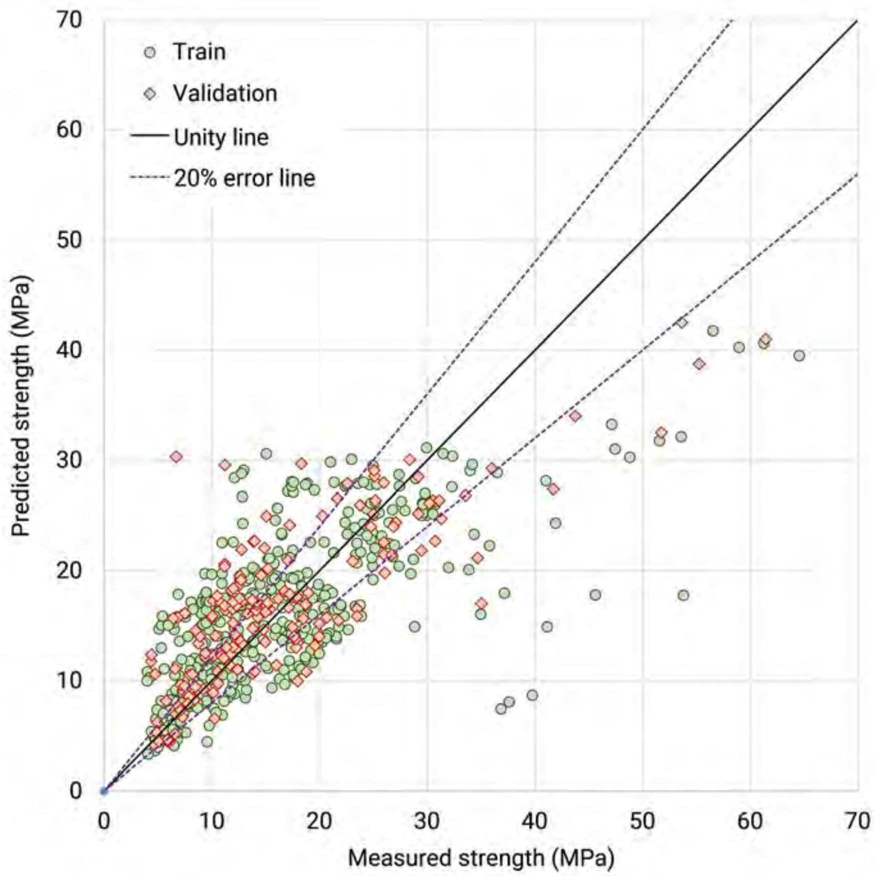

Figure 6. Correlation between measured and predicted compressive strength for linear regression model.

results indicate that the input parameters' effect on compressive varied in large ranges incongruently, displayed relatively insignificant relationships and depended on inter-dependency of confounding parameters.

4. Results and discussion

4.1. Linear regression

Equation (9) represents linear equation utilised to predict empirical correlation between compressive strength and independent variables.

$$\begin{aligned} Y = |\ \ 0.4921 \quad & 0.0055(Ca)-0.0265(Si) \\ & 0.3544(Al)-0.4030(Fe) \\ & 0.3134(Mg)-0.0916(Na.E) \quad 0.0031(Agg) \\ & 0.0837(w)-0.7435(s) \quad 0.1371(t) \end{aligned} \tag{9}$$

An analysis of correlation demonstrated a positive impact between compressive strength and variables Ca, Al, Mg, Agg, w, and t. However, an adverse effect was observed on compressive strength for variables Si, Fe, Na.E and s.

ANOVA results for linear equation can be found in Table S1. Analysis of variance (ANOVA) confirms that the equation effectively captures the association between compressive strength and independent variables. The significance of coefficient term is positively correlated with a rise in value of F and a decrease in value of p (Amini *et al.* 2008, Kalavathy M *et al.* 2009). The p-value was less than 0.05, indicating that the model possesses statistical significance with a confidence level exceeding 95% (Di Leo and Sardanelli 2020).

ANOVA results revealed that the F-value for the model was 82.69. This suggests that a considerable portion of the variation in response can be accounted for by the regression equation, indicating the model's significance. In addition, the probability $p < 0.0001$ suggested that the model was statistically significant (more than 99.9% confidence) for all input parameters.

The data were analysed to evaluate the correlation between experimental and predicted compressive strength, as shown in Figure 6. Scatter plot demonstrates a moderate dispersion of data points that align to a linear relationship. Especially, for higher compressive strength, the predicted values are underestimated for both train and validation datasets. The performance indexes of the model are summarised in Table 3. It indicates that R^2 values for prediction were compromised indicated by 0.56 and 0.65 for train and validation datasets, respectively. Furthermore, results suggest that 44.8% and 43.0% of data were within a 20% margin of error for training and validation datasets, respectively. The research reveals that selected linear model needed to be revised in accurately forecasting response variables based on experimental data.

4.2. Full quadratic

The full quadratic equation employed to predict the empirical correlation between compressive strength and independent variables in the experimental data was represented as Equation (10).

Table 3. Performance indicators for the models.

	Training dataset				Validation dataset			
	R^2	RMSE	MAE	a20	R^2	RMSE	MAE	a20
LR	0.56	6.45	4.47	44.76	0.65	6.07	4.42	43.03
FQ	0.89	3.17	2.20	72.69	0.87	3.72	2.58	69.09
ANN	0.96	1.89	1.44	85.43	0.91	2.98	2.33	67.27

$$
\begin{aligned}
Y = |\ & 59.49 \quad 0.090(Ca)-0.415(Si) \quad 0.546(Al)-0.498(Fe)-8.086(Mg) \quad 15.345(Na.E) \quad 0.042(Agg) \quad 1.140(w) \\
& -4.625(s) \quad 0.131(t) \quad 0.00004(Ca)^2-0.00089(Si)^2-0.029(Al)^2-0.072(Fe)^2-0.246(Mg)^2 \quad 0.262(Na.E)^2 \\
& -0.00002(Agg)^2 \quad 0.00049(w)^2 \quad 0.309(s)^2-0.00151(t)^2-0.00257(Ca)(Si)-0.00072(Ca)(Al)-0.010(Ca)(Fe) \\
& \quad 0.00552(Ca)(Mg) \quad 0.032(Ca)(Na.E) \quad 0.00034(Ca)(Agg)-0.00127(Ca)(w)-0.00127(Ca)(s) \quad 0.0052(Ca)(t) \\
& \quad 0.019(Si)(Al) \quad 0.021(Si)(Fe)-0.031(Si)(Mg)-0.032(Si)(Na.E) \quad 0.00007(Si)(Agg) \quad 0.00032(Si)(w) \\
& \quad 0.065(Si)(s)-0.00151(Si)(t) \quad 0.01644(Al)(Fe) \quad 0.099(Al)(Mg) \quad a40(Al)(Na.E) \quad 0.00054(Al)(Agg) \\
& -0.012(Al)(w)-0.053(Al)(s) \quad 0.00471(Al)(t) \quad 0.044(Fe)(Mg)-0.194(Fe)(Na.E)-0.00084(Fe)(Agg) \\
& \quad 0.018(Fe)(w) \quad 0.086(Fe)(s)-0.00262(Fe)(t)-0.240(Mg)(Na.E) \quad 0.00478(Mg)(Agg) \quad 0.052(Mg)(w) \\
& -0.080(Mg)(s) \quad 0.00034(Mg)(t)-0.00879(Na.E)(Agg)-0.00405(Na.E)(w)-0.164(Na.E)(s) \quad 0.00926(Na.E)(t) \\
& -0.00072(Agg)(w) \quad 0.00036(Agg)(s) \quad 0.00014(Agg)(t)-0.024(w)(s) \quad 0.00063(w)(t)-0.022(s)(t)
\end{aligned} \tag{10}
$$

ANOVA results for quadratic formula are summarised in Table S2. Analysis of variance (ANOVA) confirms that the formula effectively captures the relationship between compressive strength and independent variables. ANOVA study showed that the F-value for the model was 81.99. This indicates that quadratic formula can describe a significant amount of variability in compressive strength. These findings, in tandem with probability value of $p < 0.0001$, reinforce and indicate that the model has statistical significance. Ca, Si, Fe, Mg, w and t predominantly impact compressive strength. Supplementary model terms, identified by their p-values exceeding 0.05, did not demonstrate a significant impact.

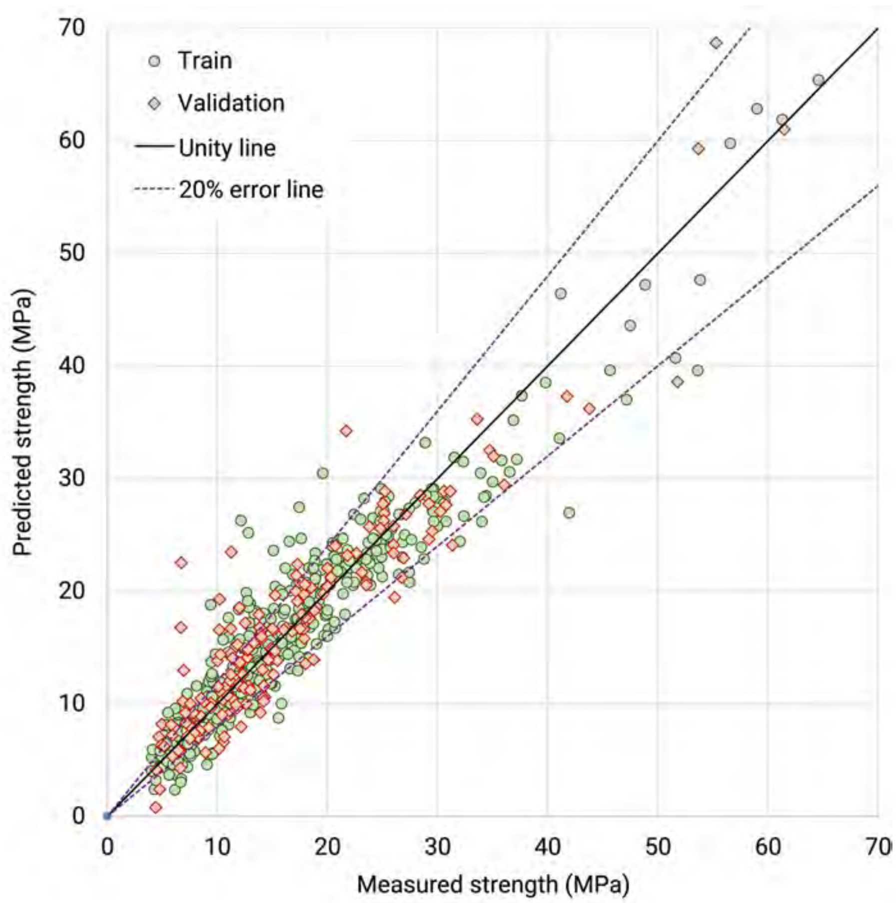

Figure 7. Correlation between measured and predicted compressive strength for full quadratic model.

Figure 7 depicts the correlation between measured and predicted compressive strengths. Scatter plot demonstrates that the data points display a strong linear relationship with a well-distributed pattern. The model performance indicators presented in Table 3 indicate that R^2 values for the train and validation datasets demonstrate high accuracy indicated by 0.89 and 0.87 for train and validation datasets, respectively. Simultaneously, the results suggest that only 72.7% and 69.1% of data were within a 20% margin of error for train and validation datasets, respectively. These numbers surpass corresponding values for the linear regression model. The analysis demonstrates that selected quadratic model was acceptable in sufficiently forecasting compressive strength using experimental data.

4.3. Artificial neural network

Fine-tuning involves making precise adjustments to get the desired outcome or degree of performance. This process is widely recognised as grid search or hyperparameter optimisation. To determine optimal values for these parameters, it is advisable to conduct an analysis using different combinations of parameters throughout the whole range. One can use cross-validation tests to determine settings that result in the highest performance (Elgeldawi *et al.* 2021). Optimal hyperparameters are contingent upon specific dataset and task at hand. Therefore, it is essential to experiment and iterate a model to determine the most optimal parameters.

Current study focused on optimising an ANN to determine optimal number of neurons and learning rate. One layer was considered sufficient. Due to its simplicity, it is more feasible to install, comprehend and interpret in comparison to intricate multi-layer networks. Neuron count reached a maximum of 15, and four distinct learning rates were employed to assess optimisation. Figure 8 depicts the relationship between R^2 and RMSE, showcasing the impact of different hyperparameters.

The optimal performance was attained with 11 neurons and a learning rate of 0.1. The optimal hyperparameters were determined by k-fold validation, with a fold count of 5. The ANN formula, including weights and biases, is shown in Equations (11)–(13).

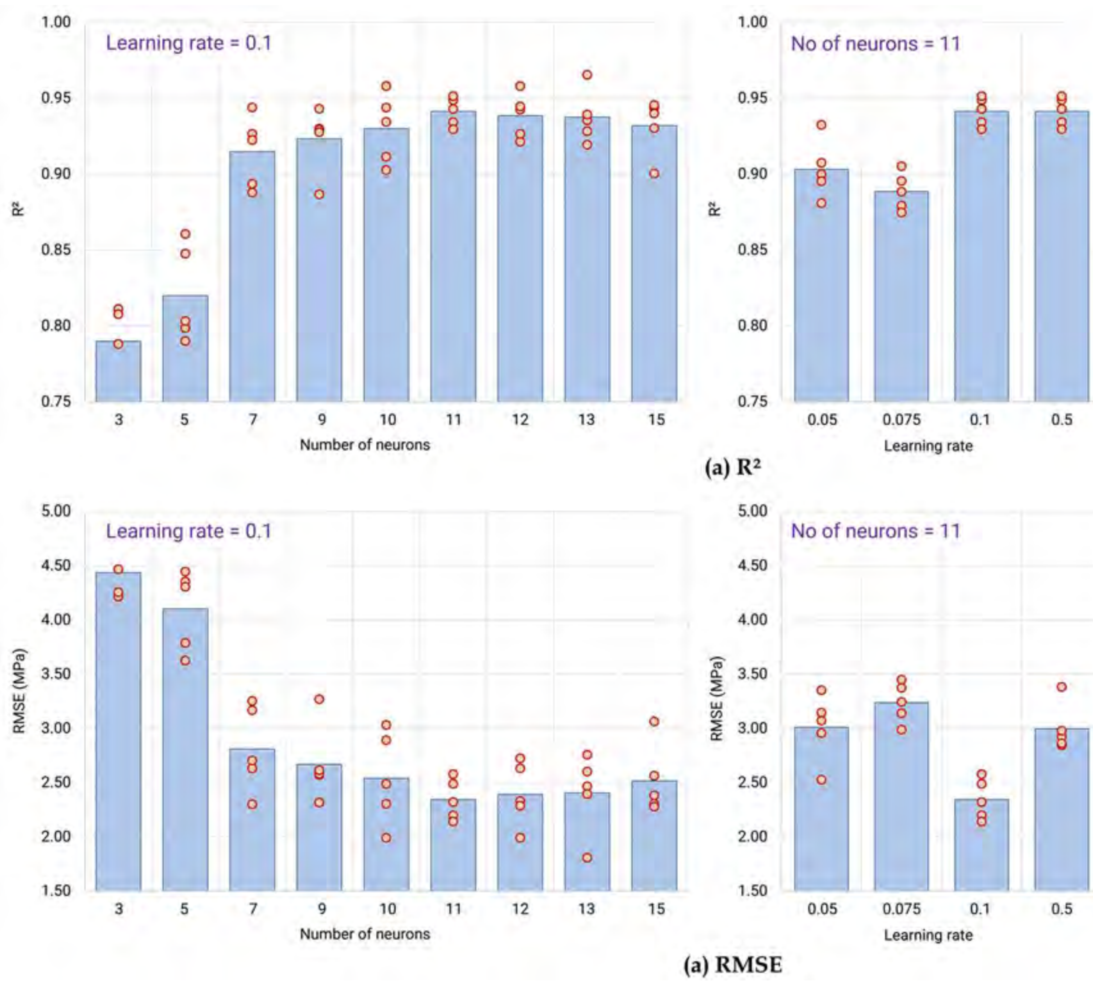

Figure 8. Effect of number of neurons and learning rate on performance of models for prediction: (a) R^2 and (b) RMSE.

$$w_i x_i \quad b_i = \begin{bmatrix} 0.0232 & \mid 0.0440 & 0.1280 & \mid 0.0992 & 0.2022 & \mid 1.0540 & \mid 0.0059 & \mid 0.0295 & \mid 0.3186 & \mid 0.0836 \\ 0.0508 & 0.0111 & \mid 0.0856 & 0.2755 & 0.5416 & 0.1835 & \mid 0.0060 & \mid 0.0299 & 0.8539 & 0.0424 \\ \mid 0.0002 & 0.0770 & 0.0564 & \mid 0.0956 & 0.3729 & \mid 0.4245 & \mid 0.0051 & \mid 0.0537 & \mid 0.7883 & \mid 0.0558 \\ \mid 0.0097 & \mid 0.0090 & 0.1317 & 0.0057 & \mid 0.5487 & \mid .0454 & \mid 0.0127 & 0.0206 & \mid 0.0328 & \mid 0.0412 \\ 0.0290 & 0.0190 & \mid 0.1045 & 0.1042 & 0.4650 & 0.0752 & 0.0097 & 0.0364 & \mid 0.1017 & 0.0026 \\ \mid 0.0291 & \mid 0.0555 & \mid 0.0459 & 0.0910 & 0.4340 & 0.0232 & 0.0119 & 0.0050 & \mid 0.0273 & 0.0998 \\ \mid 0.0085 & 0.0305 & \mid 0.0647 & 01414 & \mid 0.0603 & \mid 0.0611 & 0.0015 & 0.0474 & \mid 0.0251 & 0.0899 \\ 0.0179 & \mid 0.1054 & 0.0961 & 0.0068 & 0.0826 & 0.4013 & \mid 0.0054 & 0.0188 & 0.2193 & 0.0839 \\ \mid 0.0066 & 0.0187 & 0.1224 & \mid 0.2185 & \mid 0.3556 & 0.4239 & 0.0107 & 0.0452 & 0.1448 & 0.0626 \\ \mid 0.0109 & \mid 0.0106 & 0.0017 & 0.0788 & 0.2462 & \mid 0.6163 & 0.0118 & 0.0238 & \mid 0.3430 & 0..0105 \end{bmatrix}$$

$$\begin{matrix} CaO \\ SiO_2 \\ Al_2O_3 \\ Fe_2O_3 \\ MgO \\ Na_2O.Eq. \\ Agg \\ Water \\ Agg.\ size \\ t \end{matrix} = \begin{matrix} 16.2431 \\ \mid 15.6328 \\ 17.1812 \\ 23.7408 \\ \mid 35.3642 \\ \mid 8.2707 \\ \mid 12.3432 \\ 4.0614 \\ \mid 25.8250 \\ \mid 15.7052 \end{matrix} = \qquad (11)$$

$$\{\beta_i\} = \tanh(0.5[w_i x_i \quad b_i]) \qquad (12)$$

Each output neuron receives input from all neurons in the previous layer, not just one. Each of these inputs is multiplied by its corresponding weight before being summed up. The summed input then goes through an activation function in the output neuron. This function determines the final output value based on the weighted sum, not a simple weighted average. Here, the weights in the output layer as a set of 'filters' that transform the combined signal from the previous layer into a specific output value. If a weight is positive, it strengthens the influence of the corresponding input on output. A high positive weight for a specific input feature in the output neuron can indicate that the network has learned that this feature was important for predicting the desired output. Negative weights can weaken or even reverse the influence of an input. This can happen if the network learns that a particular feature was often associated with an opposite outcome. So the interplay between all weights and activation function in output layer determines the final output of the network. While individual weights don't directly represent a weightage in the final output value, they collectively influence the network's ability to learn complex relationships between input features and desired output.

$$\begin{aligned} f_{cr} = \mid\ & 6.1783\beta_1 \quad 9.1143\beta_2 \quad 9.4481\beta_3 \quad 12.5423\beta_4 \\ & 9.8832\beta_5 \quad 9.9292\beta_6 \quad 5.5813\beta_7 \quad 6.9791\beta_8 \\ & 8.3134\beta_9 \quad 14.0814\beta_{10} \quad 18.2102 \end{aligned} \qquad (13)$$

Results presented in Figure 9 indicate that ANN exhibits superior performance in predicting compressive strength, as observed throughout the study's training and testing datasets. The model shows an R^2 value of 0.96 for training dataset and 0.91 for validation dataset, indicating an excellent level of explained variance. RMSE is observed to be 1.89 MPa for train and 2.98 for validation dataset, representing excellent magnitude of residuals. Lastly, a20 index was measured as 85.4% for train and 67.3% for validation dataset, which implies significant model accuracy in predicting the value within the 20% error range of observed values. Compared to full quadratic model, the utilisation of ANN for training and validating data reduces RMSE by 40.4% and 19.9%, respectively. Based on the results obtained, it can be inferred that ANN model exhibits significantly superior performance compared to linear regression and full quadratic models.

4.4. Error distribution

Figure 10 displays absolute computed error (predicted – observed compressive strength) for models in log scale. This picture clearly illustrates that multiple recorded data points were considered outliers, suggesting a more significant degree of error. This can be attributed to a potential discrepancy in experimental measurement of compressive strength or to the diverse characteristics among laboratory tests conducted in the literature. ANN model exhibits a more consistent prediction accuracy than other models, demonstrating a more considerable accuracy. However, in the cases of linear regression and full quadratic models, a significant portion of larger mistakes tend to be underestimated. Therefore, assessing efficiency of the implemented predictive models by employing diverse statistical metrics and visual representations could offer a more insightful evaluation.

Figures 11 and 12 show error classification with compressive strength for full quadratic and ANN models, respectively. y-axis shows the error range (predicted – measured compressive strength) and x-axis shows measured compressive strength. For full quadratic model, higher underestimation of strength (more significant negative error: <-3 MPa) occurred more on higher compressive strength than on low-strength pervious concrete. Minimal error (-1.5–1.5 MPa) mainly occurred in low-strength pervious concrete.

For ANN model, similar to full quadratic model, higher underestimation of strength (more significant negative error: <-3 MPa) occurred more on higher compressive strength than low-strength pervious concrete. While more minor errors occurred (-0.5 to 0.5 MPa), the average strength was 13.74 MPa. Average strength for particular error ranges increased with an increase in error values.

5. Sensitivity analysis

A sensitivity analysis was performed to assess the effect of each parameter on compressive strength. A single parameter was

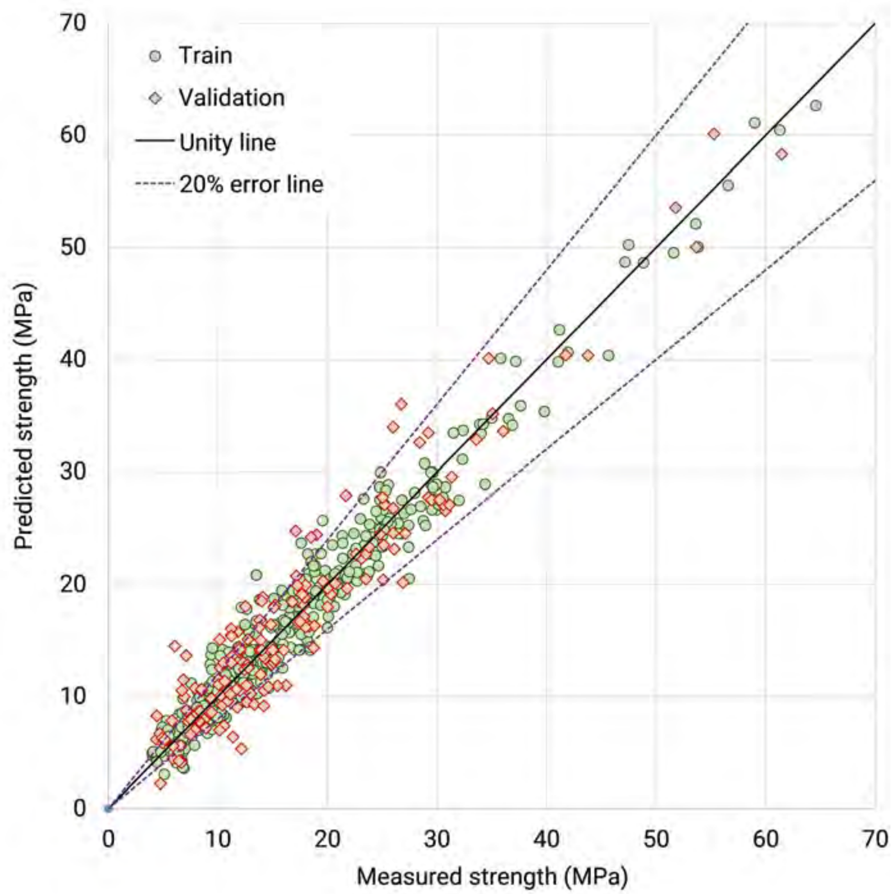

Figure 9. Correlation between measured and predicted compressive strength for ANN model.

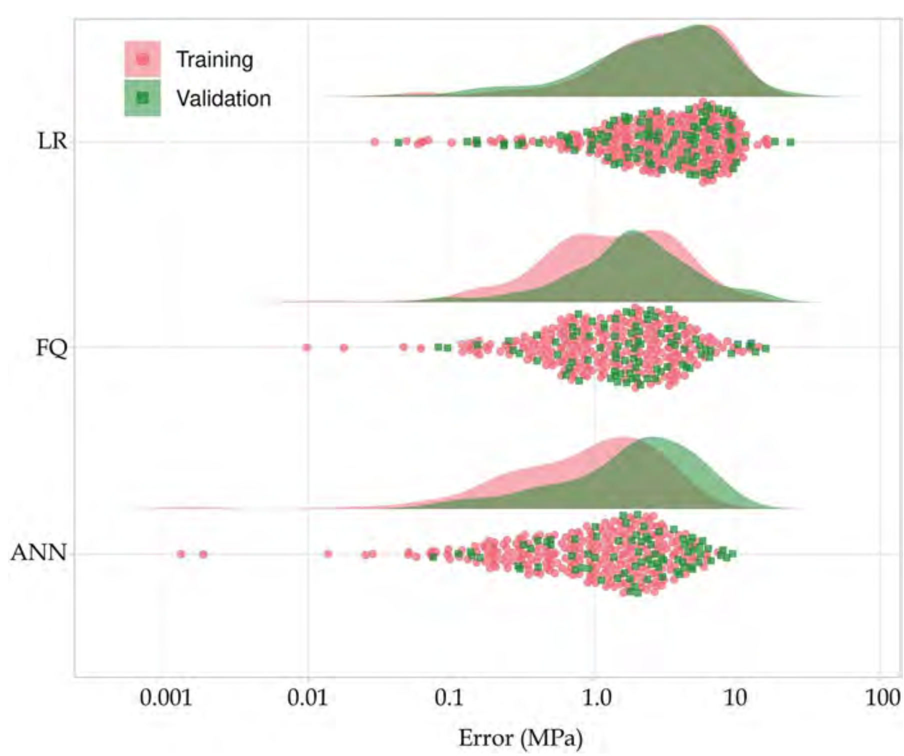

Figure 10. Error distribution of the models (in log scale).

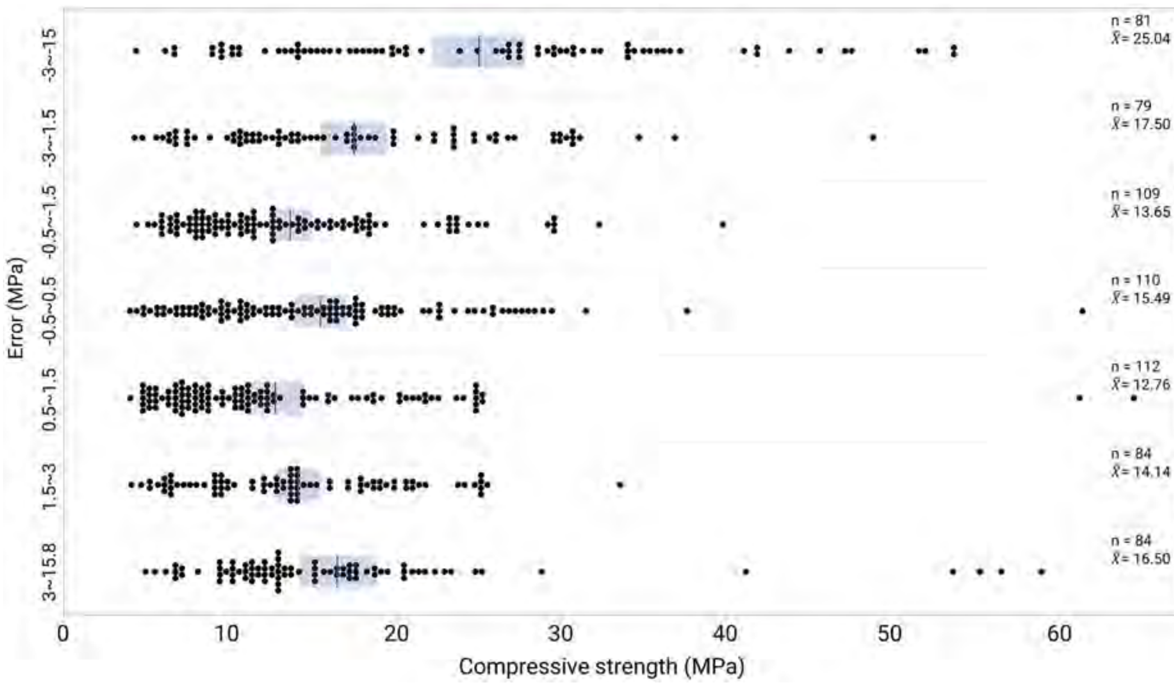

Figure 11. Error classification with compressive strength for full quadratic model.

retrieved at a time to ascertain sensitivity index of a particular parameter in a generated model. ANN model was employed to conduct a sensitivity analysis due to its superior performance in predicting compressive strength. Figure 13 displays the sensitivity results. Results suggest that Al_2O_3 is the most important and influential factor in predicting compressive strength. It is followed by the curing period and water content.

Dataset produces a SHapley Additive exPlanations (SHAP) summary plot, shown in Figure 14. This plot integrates feature relevance, represented by parameters arranged along *y*-axis, and impact on model output, indicated by SHAP values on *x*-axis. These values provide insights into the probability of predicting compressive strength. Positive SHAP values indicate a higher estimate of compressive strength. The gradient color scheme signifies varying feature values, ranging from high (red) to low (blue). According to Figure 14, Al_2O_3 was the dominant factor in predicting compressive strength. Correlation between Al_2O_3 and compressive strength is linear, as

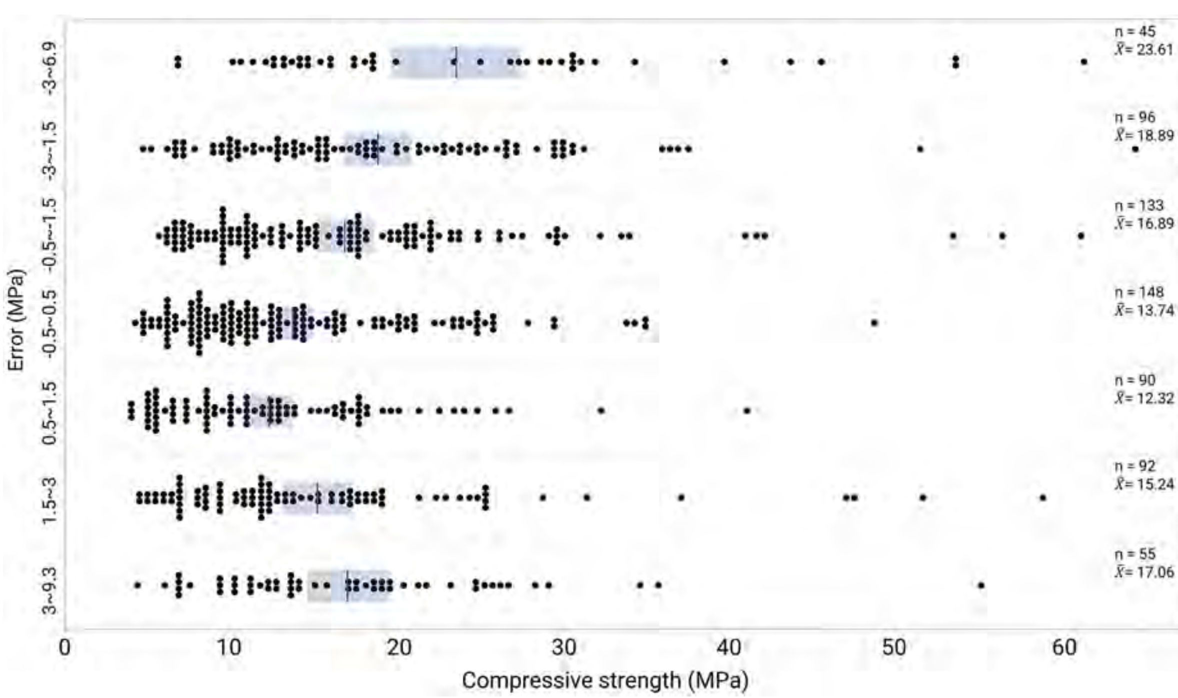

Figure 12. Error classification with compressive strength for ANN model.

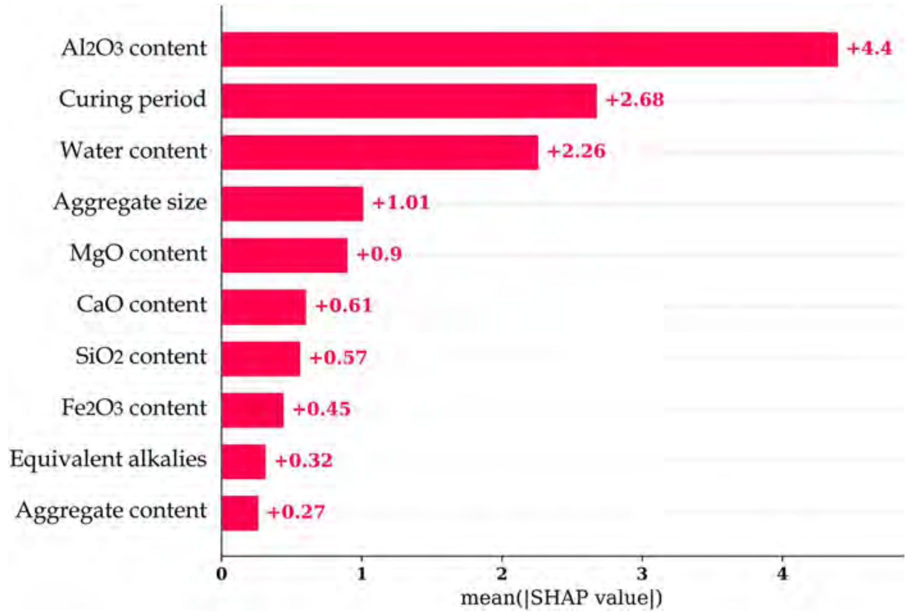

Figure 13. Mean SHAP values.

seen by a positive SHAP value associated with greater Al_2O_3 values and negative SHAP value associated with lower Al_2O_3 values. SHAP value of +10 on the right side indicates that an increase in Al_2O_3 value, as considered in this study, can lead to a 10 MPa increase in compressive strength, assuming no changes in other parameters. Similarly, a score of −12 on the left indicates that a lower concentration of Al_2O_3 in the present study can decrease compressive strength by 12 MPa. The link between curing period and CaO content has a linear trend, as both factors directly impact the compressive strength. Specifically, an increase in curing period leads to a corresponding rise in compressive strength.

Compressive strength also exhibits a linear connection with SiO_2 and equivalent alkalies. However, rise in these parameters had a detrimental impact on compressive strength. Increasing SiO_2 content in cement can adversely affect compressive strength under certain conditions. In cementitious materials, adequate quantity of formation of calcium silicate hydrate gel relies on a balanced ratio between CaO and silicon dioxide SiO_2. This ratio impacts formation of hydration products, which are the glue that binds concrete particles together (Suda *et al.* 2015). If the ratio gets too high, a phenomenon called strength retrogression can occur. At normal temperatures, excess SiO_2 acts as an inert material in the concrete mix. It doesn't participate in the hydration reaction and simply fills space without contributing to strength (Costa *et al.* 2017). This dilution effect can lower the overall compressive strength. High alkali content can accelerate early hydration process of cement, leading to a faster initial set. However, this rapid setting disrupts the formation of ideal hydration products needed

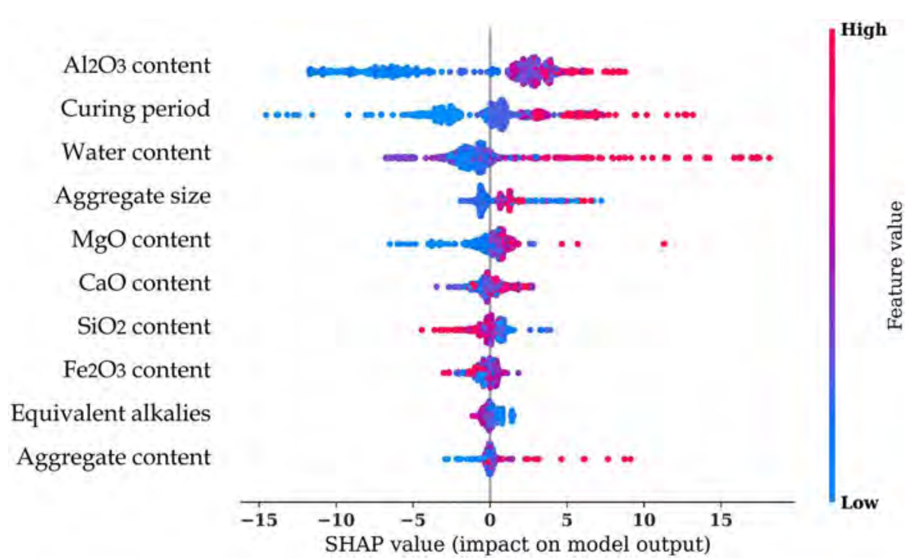

Figure 14. SHAP value (impact on model output).

for long-term strength. The resulting structure can be more porous and weaker (Fu *et al.* 2023). If mortar mix contains reactive silica, high alkalis can trigger a detrimental alkali–silica reaction. alkali–silica reaction creates a gel that expands within pervious concrete, causing cracks and significant strength loss (Panesar 2019). There is a threshold level for equivalent alkalies content. Up to a certain point, it might even slightly improve early strength. But, exceeding this level brings negative consequences for long-term strength and durability (Li *et al.* 2016). However, compared to other characteristics, the presence of equivalent alkalies has a relatively weak impact on compressive strength. Compressive strength has a non-linear correlation with other factors, such as aggregate size, Fe_2O_3 content and aggregate content.

6. Limitations of the study and machine learning models

This study demonstrates the efficacy of full quadratic regression and ANNs in predicting compressive strength of SCM-blended pervious concrete. However, some limitations inherent to the data and models employed warrant consideration:

- Data Dependence: Machine learning model accuracy hinges on the quality and quantity of training data. The current study might be limited by dataset size or diversity, potentially restricting a model's generalisability to distinct concrete mixes or real-world scenarios.
- Black Box Nature of ANNs: While ANN model performed admirably, its prediction rationale remains opaque. This 'black box' characteristic hinders the comprehension of underlying relationships between input parameters and compressive strength.
- Focus on Compressive Strength: The study solely addressed compressive strength prediction. Other critical pervious concrete properties, such as permeability and durability, were not considered. A more comprehensive model would encompass these additional factors for a holistic understanding of concrete performance.
- Chemical Composition Limitations: The study only analysed six chemical components of cementitious materials (CaO, SiO_2, Al_2O_3, Fe_2O_3, MgO, and equivalent alkali). Additional elements within these materials might also influence compressive strength, and their omission could compromise model accuracy.
- Limited Generalisability: The study might not have accounted for the influence of varying curing conditions (temperature, humidity) or the specific types of cement and SCMs used. The model's predictions could be less accurate for concrete mixes with significantly different compositions or curing procedures.

This study establishes the potential of machine learning for predicting compressive strength of SCM-blended pervious concrete. However, acknowledging these limitations and areas for improvement is crucial for the responsible and effective utilisation of this technology in the construction industry.

7. Practical implication of the proposed models

The models developed in this study have several significant practical applications that can benefit engineers and the construction industry, particularly in the context of pervious concrete.

- The prediction models enable engineers to design pervious concrete mixes with specific compressive strength requirements. By inputting the chemical composition and mix parameters, practitioners can quickly evaluate the expected strength of their concrete, allowing for optimised use of materials, which can lead to cost savings and improved performance.
- Given the environmental impact of traditional cement production, the proposed models facilitate the use of supplementary cementitious materials (SCMs). By predicting the compressive strength based on various SCMs, engineers can make informed decisions about incorporating these materials, thus contributing to greener construction practices.
- The models serve as a tool for quality assurance in the production of pervious concrete. By establishing a reliable method to predict compressive strength, they can help ensure that the concrete used in pavements meets the necessary structural requirements, ultimately enhancing the durability and lifespan of these infrastructures.
- The flexibility of the models allows for the incorporation of locally available materials and SCMs, which can vary significantly in chemical composition. This adaptability supports regional construction practices and can lead to improved performance based on local conditions.
- The findings can assist in the development of guidelines for the practical application of pervious concrete in various scenarios, such as stormwater management systems and urban infrastructure. By understanding how different variables affect strength, stakeholders can make better decisions regarding the use of pervious concrete in real-world applications.

The proposed models provide significant practical advantages for the design, production and application of pervious concrete. They not only enhance the efficiency of concrete mix design but also promote sustainability and quality in construction practices.

8. Future research directions

This study lays groundwork for advancements in pervious concrete design through machine learning. Here are some potential research directions outlining specific plans to refine the prediction model and broaden its applicability:

- Incorporating Additional Mix Design Factors: Current model focuses on general pervious concrete mix parameters. Future research should explore incorporating details like specific type of SCMs and aggregate used to enhance its accuracy and applicability across diverse construction scenarios. This could be achieved by considering the following inclusions. (i) Establishing a framework for integrating specific properties of SCMs and aggregate (e.g.

chemical composition, particle size distribution) into the machine learning model. This might involve feature engineering techniques to transform these properties into a format suitable for model training. (ii) Conducting a comprehensive study on how different SCMs and aggregate types influence the model's prediction accuracy. This would involve creating concrete mixes with various SCMs and aggregate combinations, testing their permeability and strength, and feeding the data into the model for retraining and refinement. (iii) Evaluating the feasibility of creating a model database with pre-defined properties for various SCMs and aggregate combinations. This database could be linked to prediction model, allowing users to select materials based on project specifics and obtain a more tailored prediction for permeability and strength. By incorporating these additional factors, the model can adapt to diverse construction scenarios, leading to more accurate predictions and optimised mix designs.

- Investigating Porosity, Permeability, and Long-Term Durability: While the current model focuses on compressive strength, expanding the scope to predict porosity, permeability, and long-term durability of pervious concrete formulations is crucial. Design and implement a long-term monitoring program to track performance of pervious concrete mixes under real-world conditions over an extended period. This program could involve exposing pervious concrete samples to various environmental factors like freeze–thaw cycles, deicing salts and UV radiation while measuring changes in permeability and strength. This data can then be incorporated into machine learning model as target variables. Train the model on data that includes long-term performance metrics. This will enable it to predict the expected service life of pervious concrete based on the mix design and environmental factors. Additionally, a framework within the model should be developed to predict the service life, incorporating degradation models accounting for environmental factors and material properties. With this framework, engineers can design with confidence, knowing the expected lifespan of the pervious concrete under real-world conditions. Focusing on long-term durability will lead to more robust pervious concrete formulations and contribute to their broader adoption in the construction industry.
- Real-Time Construction Applications: Integrating prediction model with real-time data acquisition during construction processes holds immense potential. Research and explore existing data acquisition technologies used in construction. This might involve investigating sensor integration during mixing to gather real-time data on material properties like moisture content and aggregate gradation. Develop an interface that seamlessly integrates the prediction model with real-time data streams. This interface could be designed for mobile devices or tablets, allowing easy access to construction.

9. Conclusion

To obtain a precise and reliable model for predicting compressive strength of pervious concrete that has been altered with various SCMs and quantities, a total of 659 data samples were gathered from published literature. These samples pertained to SCMs-modified pervious concrete with diverse chemical content, aggregate content, water content, aggregate size and curing time. Based on the gathered data and the outcomes of three distinct model methodologies, the following conclusions can be inferred:

- Statistical study reveals a moderate correlation between compressive strength and independent variables considered in the study. Full quadratic model was proposed to communicate core factors influencing pervious concrete strength. While full quadratic model provided valuable insights, the study acknowledged potential for more complex, non-linear interactions. To address this, an ANN model was also employed, as it excels in capturing these complexities that simpler models might miss.
- ANN model demonstrated superior accuracy and performance in forecasting compressive strength of pervious concrete, as determined by numerous assessment parameters, including R^2, RMSE, MAE and a20 index. The model achieved the highest R^2 values of 0.96 and 0.91 for training and validation datasets, respectively. Training set yielded the minimum RMSE and MAE values of 1.89 and 1.44 MPa, respectively. In contrast, the validation set produced RMSE and MAE values of 2.98 and 2.33, respectively.
- The sensitivity analysis demonstrates that Al_2O_3 content and curing period were the most influential parameters in forecasting compressive strength of pervious concrete. In addition, SHAP could determine if each input variable had a positive or negative impact on compressive strength. Al_2O_3, CaO, curing period and water content enhanced compressive strength of pervious concrete, while SiO_2 and equivalent alkalies had an adverse effect. There has been no discernible correlation between aggregate size and Fe_2O_3 content and compressive strength.
- The study emphasised its contribution by applying these models to a specific case of pervious concrete strength prediction. This sheds light on this increasingly important material. Additionally, comprehensive statistical analysis, including full quadratic model, serves as a valuable benchmark for future research. By comparing future models with this baseline, researchers can assess the effectiveness of new approaches.
- The practical implications of the proposed models are substantial for the construction industry. First, these models enable optimised mix design, allowing engineers to tailor pervious concrete formulations to meet specific strength requirements efficiently. Second, by facilitating the use of supplementary cementitious materials (SCMs), the models contribute to more sustainable construction practices, reducing the environmental impact associated with traditional cement production.

Furthermore, the models serve as valuable tools for quality assurance, ensuring that the produced concrete meets the necessary standards for durability and performance. They also provide guidance for incorporating locally available materials, enhancing the adaptability of pervious concrete in diverse contexts. Overall, these models not only advance the understanding of pervious concrete behavior but also offer practical solutions for engineers and stakeholders in the field, promoting the effective application of this sustainable material in real-world scenarios.

Authors' contributions

N.S.: Conceptualisation, Data curation, Analysis, Writing – original draft. P.J.: Conceptualisation, Machine learning modelling, Writing – original draft. D.N.S.: Conceptualisation, Analysis, Writing – original draft, Writing – review & editing

Consent to participate

This article does not contain any studies with human participants or animals performed by any of the authors.

Disclosure statement

No potential conflict of interest was reported by the author(s).

Data availability statement

Data can be made available on request by interested parties.

ORCID

Navaratnarajah Sathiparan http://orcid.org/0000-0001-8570-0580
Pratheeba Jeyananthan http://orcid.org/0000-0003-0476-3964
Daniel Niruban Subramaniam http://orcid.org/0000-0002-1023-1617

References

Adamu, M., *et al.*, 2021. Durability performance of pervious concrete containing rice husk ash and calcium carbide: A response surface methodology approach. *Case studies in construction materials*, 14, e00547. Available from: https://www.sciencedirect.com/science/article/pii/S2214509521000620.

Ahmad, S.A., *et al.*, 2024. Mathematical modeling techniques to predict the compressive strength of pervious concrete modified with waste glass powders. *Asian journal of civil engineering*, 25 (1), 773–785. doi:10.1007/s42107-023-00811-1.

Almeida, J.S., 2002. Predictive non-linear modeling of complex data by artificial neural networks. *Current opinion in biotechnology*, 13 (1), 72–76. Available from: https://www.sciencedirect.com/science/article/pii/S0958166902002884.

Althoey, F., *et al.*, 2023. Advancements in low-carbon concrete as a construction material for the sustainable built environment. *Developments in the built environment*, 16, 100284. Available from: https://www.sciencedirect.com/science/article/pii/S2666165923001667.

Alventosa, K.M.L., Wild, B., and White, C.E., 2022. The effects of calcium hydroxide and activator chemistry on alkali-activated metakaolin pastes exposed to high temperatures. *Cement and Concrete Research*, 154, 106742. Available from: https://www.sciencedirect.com/science/article/pii/S0008884622000333.

Amini, M., *et al.*, 2008. Application of response surface methodology for optimization of lead biosorption in an aqueous solution by *Aspergillus niger*. *Journal of hazardous materials*, 154 (1), 694–702.

Astm-C109, 2020. *Standard test method for compressive strength of hydraulic cement mortars (using 2-in. or [50-mm] cube specimens).* West Conshohocken, PA: ASTM International.

Astm-C39/39m, 2021. *Standard test method for compressive strength of cylindrical concrete specimens*. West Conshohocken, PA: ASTM International.

Baltakys, K., *et al.*, 2019. The impact of Al_2O_3 amount on the synthesis of cash samples and their influence on the early stage hydration of calcium aluminate cement. *Ceramics international*, 45 (2, Part B), 2881–2886.

Boddu, S.K., 2023. Investigating the effect of aggregate size and binder material proportion on strength and permeability of pervious concrete by statistical modeling. *In*: M.V.L.R. Anjaneyulu, M. Harikrishna, S.S. Arkatkar and A. Veeraragavan, eds. *Recent advances in transportation systems engineering and management*, Singapore: Springer Nature Singapore, 235–251.

Bs-En-12390-3, 2019. *Testing hardened concrete – compressive strength of test specimens*. London: British Standards Institution (BSI).

Bs-En-12390-4, 2019. *Testing hardened concrete - compressive strength. Specification for testing machines*. London: British Standards Institution (BSI).

Chen, X., *et al.*, 2024. Evaluating the physicochemical properties of pervious recycled aggregate concrete incorporating pozzolanic additives under acid rain attack. *Construction and building materials*, 411, 134507. Available from: https://www.sciencedirect.com/science/article/pii/S0950061823042265.

Chindaprasirt, P., *et al.*, 2008. Cement paste characteristics and porous concrete properties. *Construction and building materials*, 22 (5), 894–901. Available from: https://www.sciencedirect.com/science/article/pii/S0950061806003618.

Costa, B.L.D.S., *et al.*, 2017. Silica content influence on cement compressive strength in wells subjected to steam injection. *Journal of petroleum science and engineering*, 158, 626–633.

Di Leo, G. and Sardanelli, F., 2020. Statistical significance: *P* value, 0.05 threshold, and applications to radiomics—reasons for a conservative approach. *European radiology experimental*, 4 (1), 18. doi:10.1186/s41747-020-0145-y.

El-Hassan, H. and Kianmehr, P., 2017. Sustainability assessment and physical characterization of pervious concrete pavement made with ggbs. *MATEC web of conferences*, 120, 07001. doi:10.1051/matecconf/201712007001.

Elango, K.S., *et al.*, 2021. Properties of pervious concrete – a state of the art review. *Materials today: proceedings*, 45, 2422–2425.

Elgeldawi, E., *et al.*, 2021. Hyperparameter tuning for machine learning algorithms used for Arabic sentiment analysis. *Informatics*, 8(4), 79.

Fu, Q., *et al.*, 2023. Hydration characteristics and microstructure of alkali-activated slag concrete: A review. *Engineering*, 20, 162–179. Available from: https://www.sciencedirect.com/science/article/pii/S2095809921005221.

Gb-T50081, 2002. *Standard for test method of mechanical properties on ordinary concrete*. Beijing: China Standards Press.

Gong, K. and White, C.E., 2021. Predicting CaO–(MgO)–Al_2O_3–SiO_2 glass reactivity in alkaline environments from force field molecular dynamics simulations. *Cement and concrete research*, 150, 106588. Available from: https://www.sciencedirect.com/science/article/pii/S0008884621002374.

Harrisson, A.M., 2019. 4-constitution and specification of Portland cement. *In*: P.C. Hewlett and M. Liska, eds. *Lea's chemistry of cement and concrete*. 5th ed. Butterworth-Heinemann, Oxford, 87–155.

Hay, R. and Ostertag, C.P., 2021. New insights into the role of fly ash in mitigating alkali-silica reaction (ASR) in concrete. *Cement and concrete research*, 144, 106440. Available from: https://www.sciencedirect.com/science/article/pii/S0008884621000892.

He, Y., *et al.*, 2014. Effect of calcium–silicon ratio on microstructure and nanostructure of calcium silicate hydrate synthesized by reaction of fumed silica and calcium oxide at room temperature. *Materials and structures*, 47 (1–2), 311–322. doi:10.1617/s11527-013-0062-0.

Hillier, K., 2007. Magnesium oxide. *In*: S.J. Enna and D.B. Bylund, eds. *Xpharm: The comprehensive pharmacology reference.* New York: Elsevier, 1–4.

Hwang, S. and Yeon, J.H., 2022. Fly ash-added, seawater-mixed pervious concrete: compressive strength, permeability, and phosphorus removal. *Materials* 15(4), 1407.

Is-516, 1959. *Method of tests for strength of concrete*. New Delhi: Bureau of Indian Standards (BIS).

Joshaghani, A., *et al*., 2015. Optimizing pervious concrete pavement mixture design by using the taguchi method. *Construction and building materials*, 101, 317–325. Available from: https://www.sciencedirect.com/science/article/pii/S0950061815305158.

Kaladharan, G., *et al*., 2021. Novel admixtures for mitigation of alkali-silica reaction in concrete. *Cement and concrete composites*, 120, 104028. Available from: https://www.sciencedirect.com/science/article/pii/S0958946521000974.

Kalavathy M, H., *et al*., 2009. Modelling, analysis and optimization of adsorption parameters for h3po4 activated rubber wood sawdust using response surface methodology (rsm). *Colloids and surfaces B: biointerfaces*, 70 (1), 35–45.

Khankhaje, E., *et al*., 2018. Sustainable clean pervious concrete pavement production incorporating palm oil fuel ash as cement replacement. *Journal of cleaner production*, 172, 1476–1485.

Khuri, A. and Ja, C., 1996. *Response surfaces: designs and analyses*. New York: CRC Press.

Kumar, B.S. and Srikanth, K., 2023. A study on properties of pervious concrete with high-volume usage of supplementary cementitious materials as substitutes for cement. *Asian journal of civil engineering*, 24 (7), 1997–2009. doi:10.1007/s42107-023-00619-z.

Le, B.-A., *et al*., 2022. Predicting the compressive strength and the effective porosity of pervious concrete using machine learning methods. *KSCE journal of civil engineering*, 26 (11), 4664–4679. doi:10.1007/s12205-022-1918-z.

Li, A., *et al*., 2021. Study on the performance of pervious concrete mixed with waste glass powder. *Construction and building materials*, 300, 123997. Available from: https://www.sciencedirect.com/science/article/pii/S0950061821017578.

Li, Z., Afshinnia, K., and Rangaraju, P.R., 2016. Effect of alkali content of cement on properties of high performance cementitious mortar. *Construction and building materials*, 102, 631–639. Available from: https://www.sciencedirect.com/science/article/pii/S095006181530533X.

Mao, S., 1981. *Regression analysis and experiment design*. Shanghai: Huadong Normal University.

Mehrabi, P., *et al*., 2021. Effect of pumice powder and nano-clay on the strength and permeability of fiber-reinforced pervious concrete incorporating recycled concrete aggregate. *Construction and building materials*, 287, 122652. Available from: https://www.sciencedirect.com/science/article/pii/S0950061821004128.

Mokhtar, A. and Nasooti, M., 2020. A decision support tool for cement industry to select energy efficiency measures. *Energy strategy reviews*, 28, 100458. Available from: https://www.sciencedirect.com/science/article/pii/S2211467X20300122.

Najafi Kani, E., *et al*., 2021. The effects of nano-fe2o3 on the mechanical, physical and microstructure of cementitious composites. *Construction and building materials*, 266, 121137. Available from: https://www.sciencedirect.com/science/article/pii/S095006182033141X.

Nazeer, M., Kapoor, K., and Singh, S.P., 2023. Strength, durability and microstructural investigations on pervious concrete made with fly ash and silica fume as supplementary cementitious materials. *Journal of building engineering*, 69, 106275. Available from: https://www.sciencedirect.com/science/article/pii/S2352710223004540.

Panesar, D.K., 2019. 3-supplementary cementing materials. *In*: S. Mindess, ed. *Developments in the formulation and reinforcement of concrete*. 2nd ed. Sawston: Woodhead Publishing, 55–85.

Parimbelli, E., *et al*., 2023. Why did AI get this one wrong? — tree-based explanations of machine learning model predictions. *Artificial intelligence in medicine*, 135, 102471. Available from: https://www.sciencedirect.com/science/article/pii/S0933365722002238.

Prajapati, J.R., Pitroda, J.R., and Raval, A.D., 2019. Experimental study on pervious concrete with fly ash and metakaolin. *Journal of emerging technologies and innovative research*, 6 (5), 294–304.

Rama, M. and Shanthi, V., 2023. Study on strength, permeability and microstructure of pervious concrete blended with metakaolin. *Jordan journal od civil engineering*, 17 (1), 10–22.

Rivas Mercury, J.M., *et al*., 2006. Calcium aluminates hydration in presence of amorphous SiO_2 at temperatures below 90°C. *Journal of solid state chemistry*, 179 (10), 2988–2997.

Sarker, I.H., 2021. Machine learning: algorithms, real-world applications and research directions. *SN computer science*, 2 (3), 160. doi:10.1007/s42979-021-00592-x.

Sathiparan, N., 2021. Utilization prospects of eggshell powder in sustainable construction material – a review. *Construction and building materials*, 293, 123465.

Sathiparan, N., Dassanayake, D.H.H.P., and Subramaniam, D.N., 2024. Utilization of supplementary cementitious materials in pervious concrete: a review. *International journal of environmental science and technology*, 21 (6), 5883–5918. doi:10.1007/s13762-023-05440-4.

Sathiparan, N. and Jeyananthan, P., 2023. Prediction of masonry prism strength using machine learning technique: effect of dimension and strength parameters. *Materials today communications*, 35, 106282.

Sathiparan, N., Jeyananthan, P., and Subramaniam, D.N., 2023. Prediction of compressive strength of fly ash blended pervious concrete: a machine learning approach. *International journal of pavement engineering*, 24 (2), 2287146. doi:10.1080/10298436.2023.2287146.

Sathiparan, N., Jeyananthan, P., and Subramaniam, D.N., 2024a. Silica fume as a supplementary cementitious material in pervious concrete: prediction of compressive strength through a machine learning approach. *Asian journal of civil engineering*, 25 (3), 2963–2977. doi:10.1007/s42107-023-00956-z.

Sathiparan, N., Jeyananthan, P., and Subramaniam, D.N., 2024b. Surface response regression and machine learning techniques to predict the characteristics of pervious concrete using non-destructive measurement: ultrasonic pulse velocity and electrical resistivity. *Measurement*, 225, 114006. Available from: https://www.sciencedirect.com/science/article/pii/S0263224123015701.

Shen, P., *et al*., 2021. Conceptual design and performance evaluation of high strength pervious concrete. *Construction and building materials*, 269, 121342. Available from: https://www.sciencedirect.com/science/article/pii/S0950061820333468.

Singh, A., Biligiri, K.P., and Sampath, P.V., 2023a. Quantification of effective flow resistivity for parametric assessment of pervious concrete by using ultrasonic pulse velocity method. *Transportation research record: journal of the transportation research board*, 2677 (10), 64–78. doi:10.1177/03611981231160175.

Singh, A., Sampath, P.V., and Biligiri, K.P., 2023b. Field performance monitoring of pervious concrete pavements. *Road materials and pavement design*, 24 (12), 3013–3028. doi:10.1080/14680629.2023.2176164.

Singh, T., Siddique, R., and Sharma, S., 2022. Effectiveness of using metakaolin and fly ash as supplementary cementitious materials in pervious concrete. *European journal of environmental and civil engineering*, 26 (15), 7359–7382. doi:10.1080/19648189.2021.1988715.

Snieder, E., Shakir, R., and Khan, U.T., 2020. A comprehensive comparison of four input variable selection methods for artificial neural network flow forecasting models. *Journal of hydrology*, 583, 124299.

Stadlhofer, A. and Mezhuyev, V., 2023. Approach to provide interpretability in machine learning models for image classification. *Industrial artificial intelligence*, 1 (1), 10. doi:10.1007/s44244-023-00009-z.

Subramaniam, D.N. and Sathiparan, N., 2023. Comparative study of fly ash and rice husk ash as cement replacement in pervious concrete: mechanical characteristics and sustainability analysis. *International journal of pavement engineering*, 24 (2), 1–18. doi:10.1080/10298436.2022.2075867.

Suda, Y., Saeki, T., and Saito, T., 2015. Relation between chemical composition and physical properties of c-s-h generated from cementitious materials. *Journal of advanced concrete technology*, 13 (5), 275–290.

Sudhir Kumar, B., Srikanth, K., and Eeshwar, T., 2024. Implementation of soft computing techniques in forecasting compressive strength and permeability of pervious concrete blended with ground granulated blast-furnace slag. *Journal of soft computing in civil engineering*, 8 (2), 19–45. Available from: https://www.jsoftcivil.com/article_172918.html.

Talsania, S., Pitroda, J., and Vyas, C., 2015a. Effect of rice husk ash on properties of pervious concrete. *International journal of advanced engineering research and studies*, 4 (2), 296–299.

Talsania, S., Pitroda, J., and Vyas, C., 2015b. A review of pervious concrete by using various industrial waste materials. *Journal of internation academic research for multidisciplinary*, 4 (2), 296–299.

Tan, K.H. and Du, H., 2013. Sandless concrete with fly ash as supplementary cementing material. *Journal of sustainable cement-based materials*, 2 (3–4), 238–249. doi:10.1080/21650373.2013.827994.

Tijani, M.A., *et al*., 2019. Sustainable pervious concrete incorporating sorghum husk ash as cement replacement. *IOP conference series: materials science and engineering*, 640 (1), 012051. doi:10.1088/1757-899X/640/1/012051.

Tijani, M.A., Ajagbe, W.O., and Agbede, O.A., 2022. Combined reusing of sorghum husk ash and recycled concrete aggregate for sustainable pervious concrete production. *Journal of cleaner production*, 343, 131015.

Von Greve-Dierfeld, S., *et al*., 2020. Understanding the carbonation of concrete with supplementary cementitious materials: A critical review by Rilem tc 281-ccc. *Materials and structures*, 53 (6), 136. doi:10.1617/s11527-020-01558-w.

Wijekoon, S.H., *et al*., 2024. A mathematical model to predict the porosity and compressive strength of pervious concrete based on the aggregate size, aggregate-to-cement ratio and compaction effort. *Asian journal of civil engineering*, 25 (1), 67–79. doi:10.1007/s42107-023-00757-4.

Yaqoob, A., Musheer Aziz, R., and Verma, N.K., 2023. Applications and techniques of machine learning in cancer classification: a systematic review. *Human-centric intelligent systems*, 3 (4), 588–615. doi:10.1007/s44230-023-00041-3.

Zhang, Y., *et al*., 2022. Opening the black box: interpretable machine learning for predictor finding of metabolic syndrome. *BMC endocrine disorders*, 22 (1), 214. doi:10.1186/s12902-022-01121-4.